© 2019. Published by The Company of Biologists Ltd | Development (2019) 146, dev174128. doi:10.1242/dev.174128

RESEARCH ARTICLE

WDR62 is involved in spindle assembly by interacting with CEP170 in spermatogenesis

Yan Qin[1,2,*], Yang Zhou[3,*], Zhiming Shen[1,2,*], Binyang Xu[1,2], Min Chen[1], Yaqiong Li[1,2], Min Chen[1,2], Axel Behrens[4], Jingjing Zhou[1,2], Xin Qi[5], Wenxiang Meng[6], Yaqing Wang[6] and Fei Gao[1,2,‡]

ABSTRACT

WDR62 is the second most common genetic alteration associated with microcephaly. It has been shown that *Wdr62* is required for germ cell meiosis initiation in mice, and the majority of male germ cells are lost in the meiotic defect of first wave spermatogenesis in *Wdr62* mutants. Strikingly, in this study, we found that the initiation of meiosis following spermatogenesis was not affected and the germ cells were gradually repopulated at later developmental stages. However, most germ cells were arrested at metaphase of meiosis I and no mature sperm were detected in epididymides. Further, this study demonstrated that metaphase I arrest of *Wdr62*-deficient spermatocytes was caused by asymmetric distribution of the centrosome and aberrant spindle assembly. Also, mechanistic studies demonstrated that WDR62 interacts with centrosome-associated protein CEP170, and deletion of *Wdr62* causes downregulation of the CEP170 protein, which in turn leads to the aberrant spindle assembly. In summary, this study indicates that the meiosis of first wave spermatogenesis and the following spermatogenesis started from spermatogonium is probably regulated by different mechanisms. We also demonstrated a new function of WDR62 in germ cell meiosis, through its interaction with CEP170.

KEY WORDS: WDR62, Spindle, Spermatogenesis, Metaphase arrest, CEP170, Mouse

INTRODUCTION

Spermatogenesis is a complex process of cellular differentiation that is involved in the proliferation and differentiation of spermatogonia (Barroca et al., 2009; Brinster and Zimmermann, 1994; de Rooij and Russell, 2000), meiosis of spermatocytes and postmeiotic development of spermatids (Blobel, 2000). Meiosis is a program of two successive cell divisions preceded by one round of DNA replication that is required for the generation of haploid gametes (Braun, 2000; Yu et al., 2003). Meiotic recombination in prophase of meiosis I allows the exchange of genetic materials between paternal and maternal homologous chromosomes (Baudat et al., 2013; Kohl and Sekelsky, 2013). Homologous recombination is based on the formation of programmed DNA double-strand breaks (DSBs) and DSB repair (Ma et al., 2017; Romanienko and Camerini-Otero, 2000; Smirnova et al., 2006; Tarsounas et al., 1999). Defects in homologous recombination and DSB repair lead to meiosis arrest at the pachytene stage in spermatogenesis (Haines et al., 2015; Keeney et al., 2014; Xu et al., 2016). The spindle assembly checkpoint (SAC) is a key regulator of chromosome segregation in both mitosis and meiosis (Gorbsky, 2015). The SAC is activated when spindle assembly is disturbed or the interaction between the spindle and kinetochore of chromosomes is ruined, and prevents progression from metaphase to anaphase (Hartwell and Weinert, 1989). Disruption of the SAC results in metaphase arrest or aneuploidy gametes (Jia et al., 2013; Sacristan and Kops, 2015; Subramanian and Hochwagen, 2014; Woglar and Jantsch, 2014; Yamamoto, 2014).

The WD repeat domain 62 (*Wdr62*) gene contains 33 exons and encodes a protein containing 13 WD40-domain repeats that belongs to the WD-repeat protein family (Stirnimann et al., 2010). There are five key functional domains of WDR62 among human paralogous and orthologous proteins in various mammalian species (Cohen-Katsenelson et al., 2011). WD40 repeats at the N terminus are prominent features within proteins that mediate diverse protein-protein interactions (Stirnimann et al., 2010). The WD40-repeat domain is also required for microtubule association (Lim et al., 2015a). The MKK7β1-binding domain (MBD) is responsible for the association of WDR62 with MKK7β1 through direct protein-protein interaction and is present at the carboxyl terminus of human WDR62 (1212-1284). The JNK-binding domain (JBD), which is located at the carboxyl terminus (1291-1301), is required for c-Jun (also known as Jun) N-terminal kinase (JNK)-mediated phosphorylation of the WDR62 C terminus, which is required for spindle maintenance and mitotic progression (Bogoyevitch et al., 2012; Cohen-Katsenelson et al., 2011; Wasserman et al., 2010). The loop helix domain (LHD) is located at the carboxyl terminus of human WDR62 (1414-1520) and is necessary for homodimerization (Cohen-Katsenelson et al., 2013).

Mutation of *WDR62* is associated with microcephaly (Kousar et al., 2011; Nicholas et al., 2010; Wollnik, 2010) and with defects of neural progenitor cell development. Patients with *WDR62* mutations show a disrupted centrosome and spindle association (Farag et al., 2013). It has been reported that WDR62 is a spindle pole protein (Nicholas et al., 2010; Yu et al., 2010) and is required for the recruitment of JNK1 (Mapk8) and Aurora A (Aurka) to the spindle pole. Phosphorylation of WDR62 by JNK1 or Aurora A (Bogoyevitch et al., 2012; Xu et al., 2014) plays an opposing role in spindle maintenance and timely mitotic progression (Lim et al., 2015b). A recent study showed that WDR62 is also phosphorylated by polo-like kinase 1 (PLK1) and it is required to maintain the

[1]State Key Laboratory of Stem Cell and Reproductive Biology, Institute of Zoology, Chinese Academy of Sciences, Beijing, China 100101. [2]University of Chinese Academy of Sciences, Beijing, China. [3]State Key Laboratory of Reproductive Regulation and Breeding of Grassland Livestock, School of Life Sciences, Inner Mongolia University, Hohhot, People's Republic of China 010070. [4]CR-UK London Research Institute, London, United Kingdom. [5]The Department of Chemistry, Beijing Capital Normal University, Beijing, China 100048. [6]State Key Laboratory of Molecular Developmental Biology, Institute of Genetics and Developmental Biology, Chinese Academy of Sciences, Beijing, China 100101.
*These authors contributed equally to this work

‡Author for correspondence (gaof@ioz.ac.cn)

M.C.[1], 0000-0001-5074-2174; M.C.[1,2], 0000-0001-6577-6705; F.G., 0000-0002-4029-6411

Received 23 November 2018; Accepted 9 September 2019

Development (2019) 146, dev174128. doi:10.1242/dev.174128

orientation of the spindle in mitosis during the development of the astral spindle (Miyamoto et al., 2017).

Our recent study found that *Wdr62* plays important roles in germ cell meiotic initiation by activating JNK signaling (Zhou et al., 2018). Inactivation of *Wdr62* causes a defect in meiosis initiation and most germ cells in ovaries are lost during embryonic stage. The majority of male germ cells are lost postnatally and very few germ cells are noted at postnatal day (P)10. We also found that the defect of germ cell loss could be partially rescued by overexpression of JNK1 (Zhou et al., 2018). Interestingly, in this study, we find that the germ cells in male mice in a mouse model with only exon 2 deleted ($Wdr62^{e2-/e2-}$) are gradually repopulated at later developmental stages. However, most germ cells are arrested at the metaphase stage of meiosis I, with an asymmetrically distributed centrosome and aberrant spindle assembly. Mechanistic studies demonstrate that WDR62 interacts with centrosome-associated protein CEP170 and is required for its stability. Our study reveals a new function of *Wdr62* in spermatogenesis by regulating spindle assembly during meiosis.

RESULTS

Inactivation of *Wdr62* results in male infertility

$Wdr62^{e2-/e2-}$ mice were born at a normal Mendelian ratio, and no obvious developmental abnormalities were noted until 6 months of age. However, male $Wdr62^{e2-/e2-}$ mice were completely infertile, and the size of testes was significantly smaller than that of control mice (data not shown). To explore the reasons of male infertility, germ cells were examined at different developmental stages. MVH (DDX4)-positive germ cells were detected in both control (Fig. 1A) and $Wdr62^{e2-/e2-}$ (Fig. 1H) testes at P1, and no difference was noted. Compared with control mice (Fig. 1B-G), germ cell loss was first observed in $Wdr62^{e2-/e2-}$ mice at P3 (Fig. 1I), and very few germ cells were observed in $Wdr62^{e2-/e2-}$ mice at P5 (Fig. 1J) and P10 (Fig. 1K). Interestingly, germ cells in $Wdr62^{e2-/e2-}$ mice were gradually recovered from 2 weeks (Fig. 1L) to 3 weeks (Fig. 1M) and a large number of germ cells were observed at 6 weeks (Fig. 1N). Although germ cells were repopulated, very few round and elongated spermatids were observed in $Wdr62^{e2-/e2-}$ mice (Fig. S1C) compared with control mice (Fig. S1A), and only cell debris was observed in the epididymides of $Wdr62^{e2-/e2-}$ mice (Fig. S1D). Histological studies showed that most of the germ cells in $Wdr62^{e2-/e2-}$ mice were at the spermatocyte stage (Fig. S1C). This result was further confirmed by immunostaining of SYCP3. Only one to two layers of SYCP3-positive spermatocytes were noted in the seminiferous tubules of control mice (Fig. S1E), whereas most of the germ cells in *Wdr62*-deficient mice were SYCP3 positive (Fig. S1F).

DNA DSB repair and homologous recombination are not affected in germ cells of $Wdr62^{e2-/e2-}$ mice

To examine whether spermatocyte arrest in $Wdr62^{e2-/e2-}$ mice was due to the defect of DSB repair or homologous recombination in meiosis, immunostaining of SYCP3 was conducted to visualize the chromosome axes of primary spermatocytes. As shown in Fig. 2A, primary spermatocytes at the leptotene, zygotene, pachytene, diplotene and diakinesis (data not shown) stages were observed in both control and $Wdr62^{e2-/e2-}$ mice. The quantitative results showed that the percentage of spermatocytes in the pachytene stage was increased in $Wdr62^{e2-/e2-}$ mice (Fig. 2B). To examine whether the DSBs were properly formed, the expression of γH2AX was examined by immunofluorescence. As shown in Fig. 2C, the γH2AX signal was scattered along the chromosomes in the zygotene stage and restricted to the XY body in the pachytene and diplotene stages in both control and $Wdr62^{e2-/e2-}$ mice. Expression of DSB repair-related genes was also examined by immunostaining. Numerous RAD51-positive foci (Fig. 2D) were observed in spermatocytes in the zygotene stage, and the number was significantly reduced in the late zygotene and pachytene stages in $Wdr62^{e2-/e2-}$ mice, similar to in control mice. Statistical analysis showed that in $Wdr62^{e2-/e2-}$ spermatocytes, RAD51 signals at the pachytene stage were not affected, in comparison with those in control spermatocytes (Fig. S2K). The foci of the RPA70 (RPA1) protein (green) were located on the chromosomes (red) of both control (Fig. S2A,B) and *Wdr62*-deficient (Fig. S2C,D) germ cells at late zygotene (Fig. S2A,C) and pachytene (Fig. S2B,D) stages. A large number of DMC1-positive foci were detected on the chromosomes of both control (Fig. S2E,F) and *Wdr62*-deficient (Fig. S2G,H) germ cells at the late zygotene stage (Fig. S2E,G), and the number was dramatically reduced in the pachytene stage (Fig. S2F,H) in both control and *Wdr62*-deficient germ cells, and no difference was noted (Fig. S2L). MLH1 is a marker that indicates the completion of homologous recombination by interfering with the crossover pathway at the pachytene stage. MLH1-positive foci were observed in both control (Fig. S2I) and $Wdr62^{e2-/e2-}$ (Fig. S2J) germ cells at the pachytene stage and no difference was noted (Fig. S2M). These results indicated that the process of DSB repair and DNA homologous recombination during meiosis I were not affected in the germ cells of $Wdr62^{e2-/e2-}$ mice.

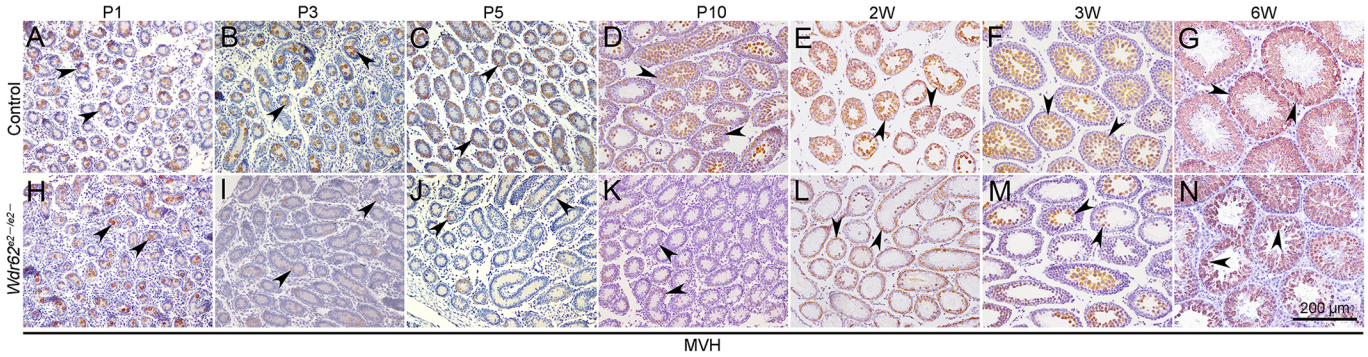

Fig. 1. Deletion of *Wdr62* resulted in germ cell loss at P3, and gradually recovered at later developmental stages. (A-N) H&E staining of control (A-G) and $Wdr62^{e2-/e2-}$ (H-N) mouse germ cells. MVH-positive germ cells (black arrowheads) were detected in both control (A) and $Wdr62^{e2-/e2-}$ (H) mice at P1. Germ cell loss was detected in $Wdr62^{e2-/e2-}$ mice at P3 (I). The number of germ cells was reduced in $Wdr62^{e2-/e2-}$ mice at P5 (J) and very few germ cells were observed at P10 (K). The number of germ cells began to increase from 2 weeks (L) to 3 weeks (M), and a large number of germ cells were observed in $Wdr62^{e2-/e2-}$ mice at 6 weeks (N). (Control, *n*=6; $Wdr62^{e2-/e2-}$, *n*=6).

Development (2019) 146, dev174128. doi:10.1242/dev.174128

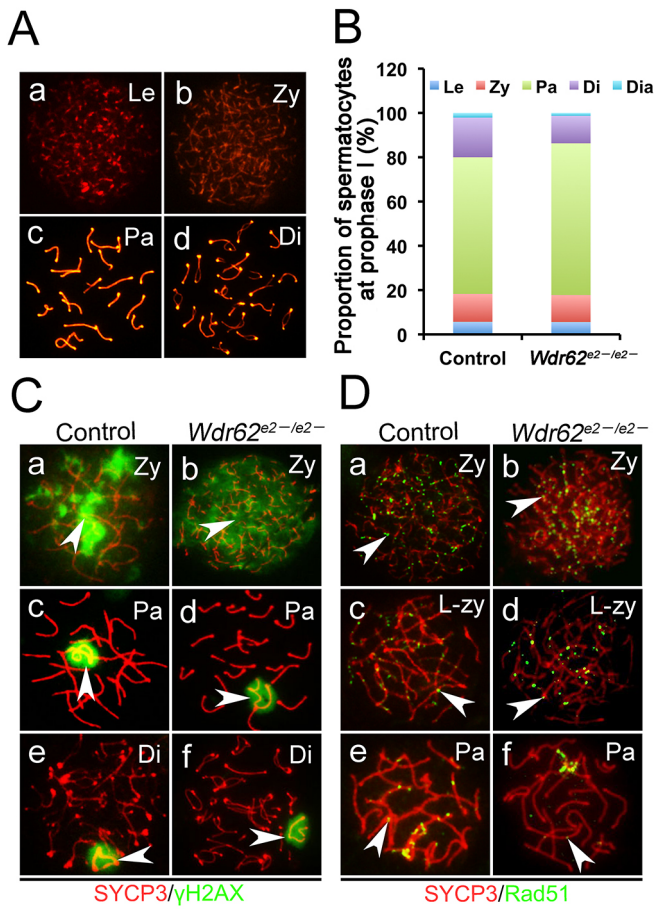

Fig. 2. DNA DSBs and DSB repair were not affected in *Wdr62*-deficient germ cells. (A) Representative synaptonemal complex at the leptotene (Aa) (control, *n*=57 cells; *Wdr62*$^{e2-/e2-}$, *n*=67 cells), zygotene (Ab) (control, *n*=127 cells; *Wdr62*$^{e2-/e2-}$, *n*=145 cells), pachytene (Ac) (control, *n*=620 cells; *Wdr62*$^{e2-/e2-}$, *n*=812 cells) and diplotene (Ad) (control, *n*=180 cells; *Wdr62*$^{e2-/e2-}$, *n*=147 cells) stages. (B) Statistical analysis of spermatocytes at prophase I. Compared with the control, the proportion of spermatocytes was increased in the pachytene stage in *Wdr62*$^{e2-/e2-}$ mice [control, 61.7%; *Wdr62*$^{e2-/e2-}$, 68.5%; degrees of freedom (d.f.)=1; χ^2=11.025] and reduced in the diplotene stage (control, 17.9%; *Wdr62*$^{e2-/e2-}$, 12.4%; d.f.=1; χ^2=13.035). The number of spermatocytes at different stages in prophase I was counted in control (*n*=1005 cells) and *Wdr62*$^{e2-/e2-}$ mice (*n*=1186 cells), and the significant difference was evaluated using the χ^2 test: χ^2>3.84 was considered as significant. (C) Expression of γH2AX (green, white arrowheads) was not changed in *Wdr62*-deficient germ cells (Cb,Cd,Cf) compared with control germ cells (Ca,Cc,Ce). (D) Expression of RAD51 (green, white arrowheads) in *Wdr62*-deficient germ cells (Db,Dd,Df) was similar to that of control germ cells (Da,Dc,De). Di, diplotene; Dia, diakinesis; Le, leptotene; L-zy, late zygotene; Pa, pachytene; Zy, zygotene.

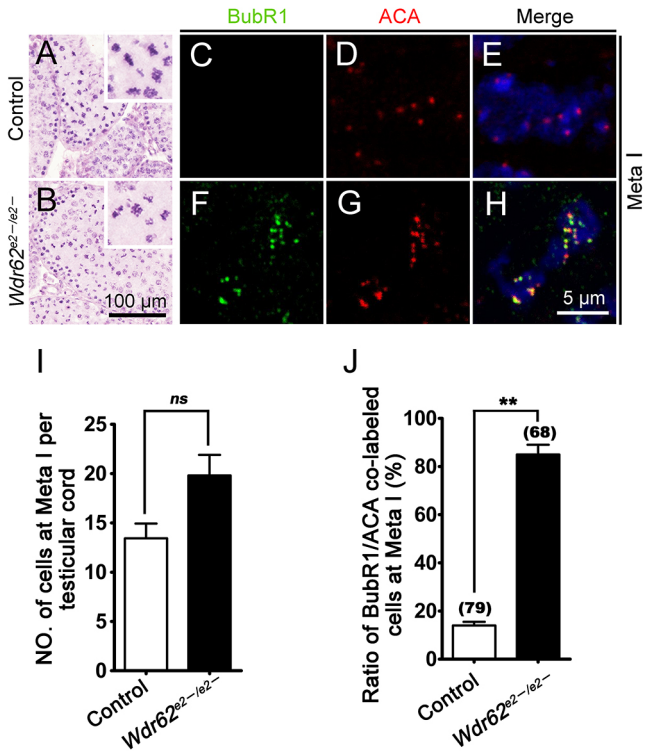

Fig. 3. Germ cells in *Wdr62*-deficient mice were arrested in the metaphase I stage of meiosis. (A,B) Spermatocytes in the metaphase I (Meta I) stage of meiosis were observed in both control (A, inset) and *Wdr62*$^{e2-/e2-}$ (B, inset) mice at 5 weeks of age. (C-H) Expression of BUBR1 and ACA was examined by immunofluorescence. The ACA protein (red) was observed at the kinetochore in both control (D) and *Wdr62*-deficient (G) spermatocytes at the Meta I stage. Numerous BUBR1-positive foci (green) were detected in *Wdr62*-deficient spermatocytes (F) at the Meta I stage and co-localized with the ACA protein (H). However, very few BUBR1-positive foci were detected in control germ cells at this stage (C,E). (I) Quantification of the number of spermatocytes at Meta I in different testicular cords from three independent testes. The number of spermatocytes was increased in *Wdr62*$^{e2-/e2-}$ mice, but not significantly. Data are mean±s.e.m. of the spermatocytes of three testes (ns, *P*>0.05; Student's *t*-test, two-tailed). (J) Quantification of the number of spermatocytes with ACA-positive signals, BUBR1 and ACA double-positive signals at Meta I in control and *Wdr62*$^{e2-/e2-}$ testes from three samples. The ratio of BUBR1 and ACA co-labeled spermatocytes at Meta I was significantly increased in *Wdr62*$^{e2-/e2-}$ mice. Data are mean±s.e.m. from one experiment with the indicated number of spermatocytes (control, *n*=79 cells; *Wdr62*$^{e2-/e2-}$, *n*=68 cells). Control, 18%; *Wdr62*$^{e2-/e2-}$, 85%. **P<0.01 (Student's *t*-test).

Germ cells in *Wdr62*-deficient mice are arrested at the metaphase I stage of meiosis

Spermatocytes at metaphase I of meiosis were observed (Fig. 3B, inset) and quantified (Fig. 3I) in the seminiferous tubules of *Wdr62*$^{e2-/e2-}$ mice at 5 weeks of age compared with control (Fig. 3A). To test whether germ cells in *Wdr62*-deficient mice were arrested at metaphase I of meiosis, the expression of BUBR1 (BUB1B) and anti-centromere antibody (ACA) was examined by immunofluorescence. BUBR1 is the core protein of the SAC and is recruited to the kinetochores when the spindle is improperly assembled (Fan, 2010; Wei et al., 2010). ACA protein was located at the kinetochore in both control (Fig. 3D) and *Wdr62*-deficient (Fig. 3G) spermatocytes at the metaphase I stage. Many BUBR1-positive foci were detected in *Wdr62*-deficient (Fig. 3F) spermatocytes at metaphase I stage and co-localized with ACA protein (Fig. 3H). Very few BUBR1-positive foci were detected in control germ cells at this stage (Fig. 3C,E). Quantitative analysis showed that the percentage of BUBR1 and ACA co-labeled spermatocytes in metaphase I was dramatically increased in *Wdr62*$^{e2-/e2-}$ mice (Fig. 3J). These results indicated that *Wdr62*-deficient germ cells were arrested at the metaphase I stage.

Aberrant spindle assembly in spermatocytes of *Wdr62*$^{e2-/e2-}$ mice at the metaphase I stage

It has been reported that activation of the SAC is closely related to aberrant assembly of the spindle (Xiong et al., 2008; Xu et al., 2012; Yuan et al., 2010). The morphology of the spindle was examined by immunostaining with an anti-α-tubulin antibody. As shown in Fig. 4, the spindles in spermatocytes from control mice in

Development (2019) 146, dev174128. doi:10.1242/dev.174128

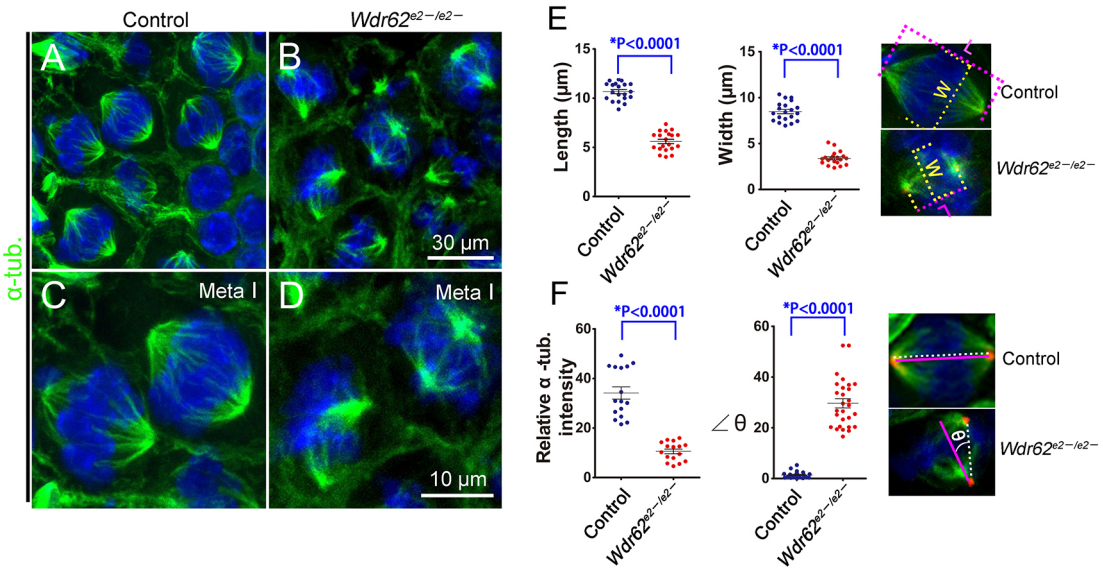

Fig. 4. Aberrant spindle assembly in spermatocytes of *Wdr62*$^{e2-/e2-}$ mice at metaphase I stage. (A-D) Well-organized and symmetrically located α-tubulin-positive spindles (green) were observed in spermatocytes at the metaphase I (Meta I) stage in control testes (A,C). Most of the spindles were disrupted in *Wdr62*-deficient germ cells (B,D). (E,F) The average length (L) and width (W) of the spindle in *Wdr62*-deficient germ cells were dramatically reduced compared with controls (E) (control, *n*=20; *Wdr62*$^{e2-/e2-}$, *n*=20). The relative α-tubulin intensity was also significantly reduced (control, *n*=16 cells; *Wdr62*$^{e2-/e2-}$, *n*=16) and the intersection angle (∠θ) between the spindle polarity axis (red line) and planar orientation (white dotted line) was significantly increased (control, *n*=25; *Wdr62*$^{e2-/e2-}$, *n*=28) in *Wdr62*-deficient spermatocytes (F). Data are mean±s.e.m. from one experiment with the indicated number of spermatocytes at Meta I. **P*<0.0001 (Student's *t*-test, two-tailed).

metaphase I were well organized, with symmetric spindle poles (Fig. 4A,C). By contrast, spindles in spermatocytes from *Wdr62*$^{e2-/e2-}$ mice were severely disrupted, with asymmetrically located spindle poles (Fig. 4B,D). The average length and width of the spindles were dramatically reduced in *Wdr62*$^{e2-/e2-}$ spermatocytes compared with those of control mice (Fig. 4E). In addition, the relative intensity of α-tubulin was also significantly reduced in *Wdr62*$^{e2-/e2-}$ mice. The spindle polarity axis of spermatocytes during the metaphase I stage in *Wdr62*-deficient mice exhibited a substantial rotation from the planar orientation (as noted by γ-tubulin and α-tubulin staining). The intersection angle between the spindle polarity axis and planar orientation was significantly increased in *Wdr62*-deficient spermatocytes (Fig. 4F). Very few spermatocytes at anaphase I were observed in *Wdr62*$^{e2-/e2-}$ mice compared with control (Fig. S3A), but the intermediate tubules were severely disrupted (Fig. S3B). High magnification images showed that homologous chromosomes moved to bipolarity in control mice (Fig. S3C) during anaphase I; however, owing to the destruction of the spindle in *Wdr62*$^{e2-/e2-}$ mice (Fig. S3D), the separation of homologous chromosomes was perturbed. These results indicate that the assembly and positioning of the spindle during metaphase I were disrupted in *Wdr62*-deficient germ cells, which most likely caused metaphase I arrest.

The positioning of the centrosome during metaphase I is disturbed in spermatocytes of *Wdr62*$^{e2-/e2-}$ mice

To examine the polarity and morphology of the centrosome, pericentriolar material (PCM) was labeled with γ-tubulin. As shown in Fig. 5, an asymmetric location of γ-tubulin-positive PCM was observed in most *Wdr62*-deficient germ cells (Fig. 5C,D) compared with control (Fig. 5A,B). Also, very little multipolar PCM was observed in a small proportion of *Wdr62*-deficient germ cells (Fig. 5E,F). The results of quantitative analysis showed that the number of germ cells with asymmetric PCM was dramatically increased in *Wdr62*$^{e2-/e2-}$ mice (Fig. 5G).

To determine whether *Wdr62* was also involved in centrosome polarity and spindle assembly in somatic cells, mouse embryonic fibroblast (MEF) cells from control and *Wdr62*$^{e2-/e2-}$ mice were cultured *in vitro*, the proliferation (Fig. S4A) and spindle

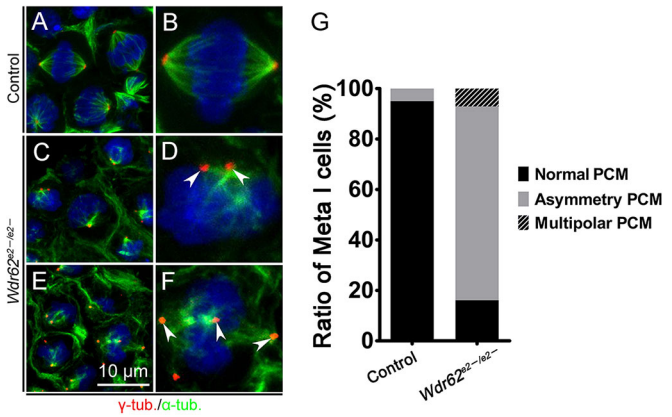

Fig. 5. The positioning of the centrosome was disturbed in *Wdr62*-deficient germ cells. (A-F) A well-organized spindle (green; α-tubulin) and symmetrically distributed centrosomes (red; γ-tubulin) were observed in control germ cells (A,B). The centrosomes were asymmetrically distributed in most *Wdr62*-deficient germ cells (C,D; white arrowheads), and a multipolar centrosome was also observed in *Wdr62*-deficient germ cells (E,F; white arrowheads). B,D,F show magnified detail of A,C,E, respectively. (G) Quantification of spermatocytes in the metaphase of meiosis I (Meta I) stage from at least four testes showing that the majority of spermatocytes displayed abnormal localization of the centrosome. Normal PCM (control, *n*=57, 95%; *Wdr62*$^{e2-/e2-}$, *n*=9, 16.1%); asymmetry PCM (control, *n*=3, 5%; *Wdr62*$^{e2-/e2-}$, *n*=43, 76.8%); multipolar PCM (control, *n*=0; *Wdr62*$^{e2-/e2-}$, *n*=4, 7.1%). We counted a similar number of spermatocytes with γ-tubulin-positive centrosomes in control (*n*=60) and *Wdr62*$^{e2-/e2-}$ (*n*=56) testes and calculated the percentage of spermatocytes with normal, asymmetric and multipolar PCM, respectively. Data are from one experiment with the indicated ratio of spermatocytes (*P*<0.001; Student's *t*-test, two-tailed).

Development (2019) 146, dev174128. doi:10.1242/dev.174128

morphology (Fig. S4B) were examined. The results of the MTT assay showed that the proliferative rate of *Wdr62*$^{e2-/e2-}$ MEF cells was comparable with that of control MEF cells. No defect of centrosome positioning or spindle assembly was observed in *Wdr62*$^{e2-/e2-}$ MEF cells (Fig. S4Bg-Bl). These results suggest that the long isoform of *Wdr62* is not expressed in somatic cells and thus not involved in spindle assembly of somatic cells.

WDR62 is abundantly expressed in spermatocytes/round spermatids and interacts with CEP170

To explore the regulatory mechanisms of WDR62 in germ cell meiosis, a hemagglutinin (HA)-tagged *Wdr62* knock-in mouse model (hereafter referred to as *Wdr62-HA*) was generated using CRISPR/Cas9 technology (Fig. S5A). The HA signal was detected in the cytoplasm of spermatocytes and round spermatids (Fig. S5C, arrowheads and arrows, respectively) in *Wdr62-HA* mice, but not in the control testes (Fig. S5B). A ∼200-kD band was detected in the testes of *Wdr62-HA* mice by western blotting using both anti-HA and anti-WDR62 antibodies (Fig. S5D). These results indicate that the endogenous long isoform of WDR62 protein in *Wdr62-HA* mice was recognized by the anti-HA antibody. Then, the subcellular localization of WDR62 in spermatocytes was examined by double-staining of HA (Fig. S5E,I), γ-tubulin (Fig. S5F) and α-tubulin (Fig. S5J) at metaphase I (Fig. S5G,K). We found that WDR62 was co-localized with the γ-tubulin-positive centrosome (Fig. S5H) and α-tubulin-positive spindle (Fig. S5L).

We further examined the expression of WDR62 protein in other tissues (Fig. S6B). Interestingly, the ∼200-kD band was only detected in testes with anti-HA antibody, not in other tissues, including the brain. By contrast, a smaller band (∼170-kD) was detected in the brain and ovary by an anti-Wdr62 antibody and was absent in adult testes. Then, we examined the expression of WDR62 protein in testes at different developmental stages (Fig. S6A). Both the small and large isoforms were detected in the control testes at 3 weeks, whereas only the large band was absent in *Wdr62*$^{e2-/e2-}$ testes. Only the large isoform was expressed in testes at 3 months and was absent in *Wdr62*$^{e2-/e2-}$ testes. All of these results suggest that different isoforms of WDR62 are expressed in testes and other tissues. The large isoform (∼200-kD) was expressed in adult testes, and the small isoform (∼170-kD) was expressed in the brain and other tissues.

To further explore the mechanistic basis of WDR62 in regulating the polarity of the centrosome and spindle assembly, WDR62-interacting proteins were screened by co-immunoprecipitation (Co-IP) and iTRAQ mass spectrometry analyses using testes from adult control and *Wdr62-HA* mice. Notably, several classes of proteins were pulled down by the anti-HA antibody, including centrosome-related protein, PIWI-like protein, motor-related protein and APC-related protein (Fig. 6A). Among others, CEP170 is a centrosome-associated protein that has been reported to be involved in spindle assembly (Welburn and Cheeseman, 2012). For a more detailed characterization of the subcellular localization of WDR62

A

Table 1 Protein detected in the testis of adult *Wdr62-HA* mice by iTRAQ mass spectrometry analysis

Functional classification	Protein name
Centrosome-related protein	Centrosomal protein of 170 Isoform 2 of Centrosomal protein of 72
PIWI-like protein	Piwi-like protein 1 Piwi-like protein 2
RNA-binding protein	ATP-dependent RNA helicase DDX17 Inosine-5'-monophosphate dehydrogenase 2
Motor-related protein	Myosin-11 Myosin-10 Myosin-9
APC-related protein	Trim33

B

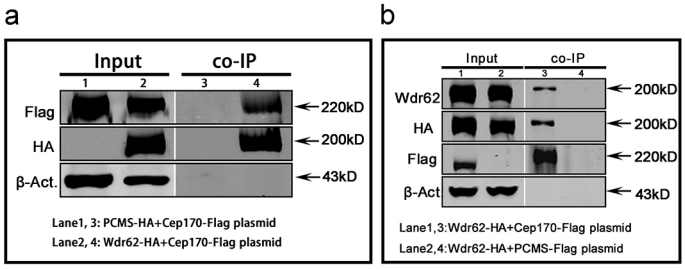

C

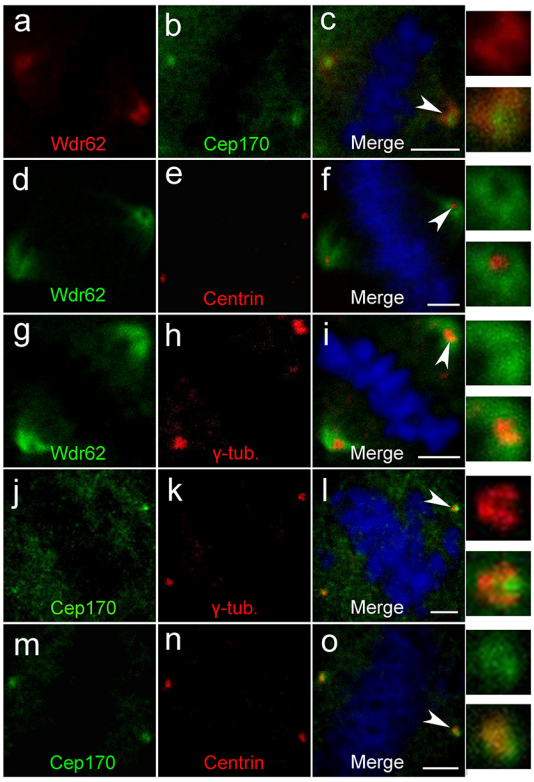

Fig. 6. WDR62 interacted with centrosome-associated protein CEP170. (A) The list of WDR62-interacting proteins identified by Co-IP and mass spectrometry (iTRAQ) analysis using testes from 2-month-old mice. The proteins listed in the table were only detected in *Wdr62-HA* mice, not in control mice. (B) Western blot showing that WDR62 and CEP170 were mutually pulled down by overexpression of HA-tagged WDR62 and Flag-tagged CEP170 in 293 cells. Input and Co-IP were loaded with ∼16 µg and ∼500 µg protein, respectively. (C) HA-tagged WDR62 and Flag-tagged CEP170 were overexpressed in HeLa cells, and the subcellular locations of WDR62, CEP170, centrin and γ-tubulin were examined by immunofluorescence. White arrowheads indicate merged signals. Panels on right show magnified details of the arrowheads. Scale bars: 3 µm.

Development (2019) 146, dev174128. doi:10.1242/dev.174128

and CEP170, immunofluorescence was performed in CEP170- and WDR62-overexpressing HeLa cells. WDR62 (Fig. 6Cg) was co-localized with γ-tubulin (Fig. 6Ci), but the signal was broader than that of γ-tubulin (Fig. 6Ch). The centrin signal was surrounded by the WDR62 protein, but these two proteins were not overlapped (Fig. 6Cf). The CEP170 protein partially overlapped with the centrin protein (Fig. 6Co) and WDR62 (Fig. 6Cc).

To further confirm the interaction between WDR62 and CEP170 proteins, Flag epitope-tagged CEP170 and HA epitope-tagged WDR62 were overexpressed in 293 cells. Co-IP experiments showed that the CEP170 protein was pulled down by the anti-HA antibody and that WDR62 was pulled down by the anti-Flag antibody (Fig. 6B). The interaction of WDR62 and CEP170 protein was also confirmed by Co-IP experiments using testes from *Wdr62-HA* mice. As shown in Fig. 7A, endogenous CEP170 protein was pulled down by the anti-HA antibody. The results of immunostaining showed that CEP170 protein was localized at the centrosome in spermatocytes of control testes (Fig. 7Ca, arrowheads), whereas it was virtually absent in spermatocytes of *Wdr62*-deficient testes (Fig. 7Cb). We also found that the protein level of CEP170 was dramatically reduced in *Wdr62*-deficient testes (Fig. 7B). To determine whether *Wdr62* depletion destabilizes CEP170 positioning and disrupts the spindle formation in mitotic cells, the CEP170 positioning (Fig. S7B,F) and spindle morphology (Fig. S7A,E) were examined in MEF cells from control (Fig. S7C,D) and $Wdr62^{e2-/e2-}$ mice (Fig. S7G,H). No defect in CEP170 expression (Fig. S7F) and spindle assembly (Fig. S7E) was observed in $Wdr62^{e2-/e2-}$ MEF cells (Fig. S7H). These results indicated that the inactivation of *Wdr62* does not cause instability of CEP170 protein in somatic cells. Given that CEP170 is an important centrosome protein, the defect of centrosome positioning and aberrant spindle assembly in *Wdr62*-deficient germ cells were most likely due to downregulation of the CEP170 protein in germ cells.

The defect in germ cell survival in $Wdr62^{e2-/e2-}$ mice is partially rescued by JNK1 overexpression, but the defect in spermatogenesis is not rescued

It has been reported that WDR62 is involved in spindle assembly in neural progenitor cells via activating JNK signaling (Shohayeb et al., 2017). And our recent study also finds that WDR62 is involved in germ cell meiosis initiation via activating JNK signaling (Zhou et al., 2018). To test whether WDR62 involvement in spindle assembly in germ cell meiosis is also JNK signaling dependent, $Wdr62^{e2-/e2-}$; $CAJNK1^{+/flox}$; *Tnap-Cre* mice (hereafter referred to as *Tnap-Cre* rescued mice) were generated. In this mouse model, constitutively activated JNK1 was specifically expressed in *Wdr62*-deficient germ cells from approximately embryonic day (E)8.5. As shown in Fig. 8, a few MVH and PLZF (Zbtb16) double-positive germ cells were observed in a small portion of seminiferous tubules in $Wdr62^{e2-/e2-}$ mice at P10 (Fig. 8D) compared with control (Fig. 8A), and the number of MVH and PLZF double-positive germ cells was significantly increased in the testes of *Tnap-Cre* rescued mice (Fig. 8G,J) at this stage. At two months of age, MVH-positive (green) and PLZF-positive (red) germ cells were noted in testes of control (Fig. 8B), $Wdr62^{e2-/e2-}$ (Fig. 8E) and *Tnap-Cre* rescued (Fig. 8H) mice. The number of MVH-positive germ cells was significantly increased in *Tnap-Cre* rescued mice (Fig. 8H,J) compared with $Wdr62^{e2-/e2-}$ mice (Fig. 8E,J). Mature sperm were observed in the epididymides of control mice (Fig. 8C), but not in $Wdr62^{e2-/e2-}$ (Fig. 8F) and *Tnap-Cre* rescued (Fig. 8I) mice. Aberrant spindle assembly was also observed in most spermatocytes at metaphase I in *Tnap-Cre* rescued mice (Fig. S8C,F), which was consistent with $Wdr62^{e2-/e2-}$ (Fig. S8B,E) mice. The quantified analysis (Fig. S8G) showed that the average length and width of the spindles or the relative intensity of α-tubulin were dramatically reduced in $Wdr62^{e2-/e2-}$ and *Tnap-Cre* rescued spermatocytes compared with those of control mice (Fig. S8A,D). To further test whether the defect of spindle assembly in $Wdr62^{e2-/e2-}$ mice can be rescued by activating JNK signaling at a later developmental stage, $Wdr62^{e2-/e2-}$; $CAJNK1^{+/flox}$; *Stra8-Cre* mice were generated. In this mouse model, JNK1 was specifically overexpressed in germ cells of $Wdr62^{e2-/e2-}$ mice at ∼P5. The results of Hematoxylin and Eosin (H&E) staining showed that the spermatogenesis defect was not rescued in this mouse model (Fig. S9) at 2 months of age. We propose that the lost MVH-positive cells at P10 were the germ cells which directly start meiosis from gonocytes, and the remaining PLZF and MVH co-labeled cells were the spermatogonium transformed from the small number of gonocytes, which will start the following wave of spermatogenesis. All of these results indicate that the survival of germ cells in $Wdr62^{e2-/e2-}$ mice was dependent on JNK signaling, whereas the function of WDR62 in spindle assembly during spermatogenesis was independent of JNK signaling.

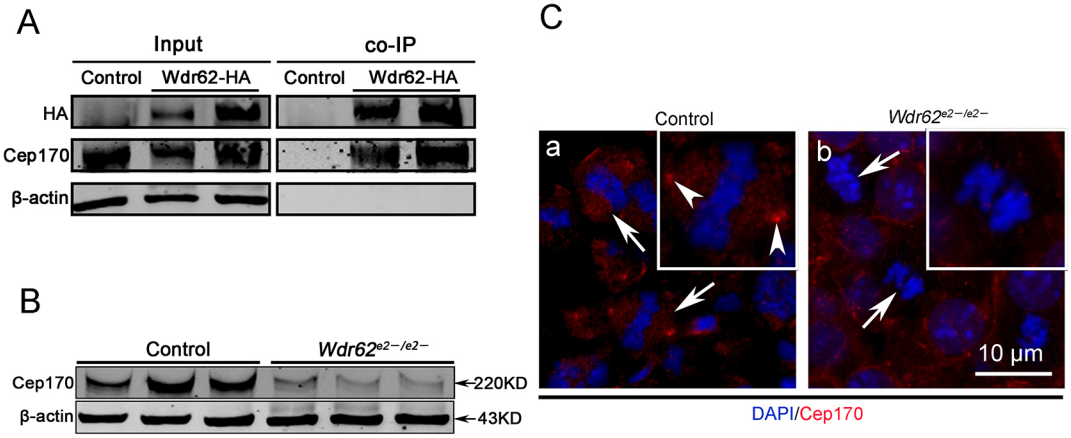

Fig. 7. WDR62 interacted with CEP170 in *Wdr62-HA* mice. (A) Western blot showing that CEP170 protein was pulled down by anti-HA antibody in testes of *Wdr62-HA* mice. (B) The protein level of CEP170 was dramatically reduced in *Wdr62*-deficient testes. (C) Immunofluorescence showing that CEP170 protein was localized at the centrosome in spermatocyte of control testes (Ca, white arrowheads), whereas it was virtually absent in spermatocytes of *Wdr62*-deficient testes (Cb). Insets show magnified detail of main panel. White arrows show the spermatocytes.

Development (2019) 146, dev174128. doi:10.1242/dev.174128

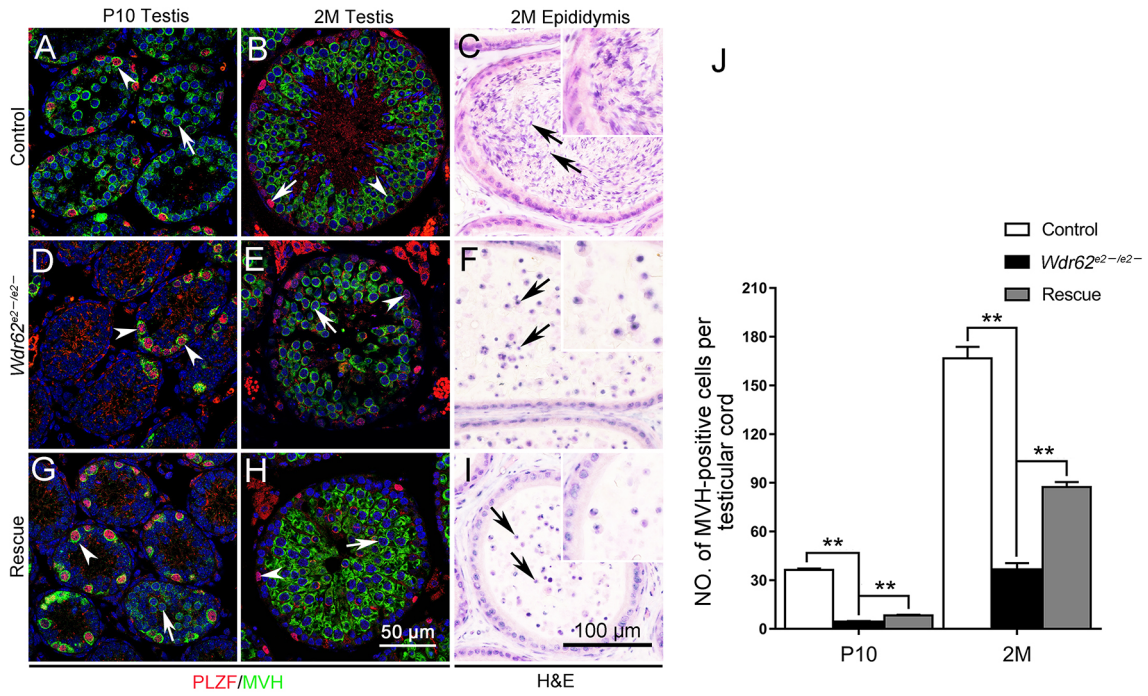

Fig. 8. The germ cell loss in *Wdr62*$^{e2-/e2-}$ mice was partially rescued by JNK1 overexpression, whereas the defect in spermatogenesis was not rescued. (A-I) Immunofluorescence showing PLZF (red) and MVH (green) double-staining in germ cells in testes of control (A), *Wdr62*$^{e2-/e2-}$ (D) and *Tnap-Cre*-rescued (G; rescue) mice at P10 and control (B), *Wdr62*$^{e2-/e2-}$ (E), and *Tnap-Cre* rescued (H) mice at 2 months of age. White arrows indicate MVH-positive cells, white arrowheads indicate MVH- and PLZF-double positive cells. H&E staining showed numerous mature sperm (black arrows) in the epididymides of control mice (C), but only cell debris was observed in the epididymides of *Wdr62*$^{e2-/e2-}$ (F) and *Tnap-Cre*-rescued (I) mice. (Control, *n*=6; *Wdr62*$^{e2-/e2-}$, *n*=6). (J) Quantification showing that the number of MVH-positive cells in each seminiferous tubule of *Tnap-Cre*-rescued mice was significantly increased at P10 and 2 months compared with *Wdr62*$^{e2-/e2-}$ mice. P10 mice: control (*n*=141), 36.31±0.9074; *Wdr62*$^{e2-/e2-}$ (*n*=265), 4.54±0.3517; *Tnap-Cre* rescue (*n*=278), 8.284 ±0.4729. 2M mice: control (*n*=81), 166.7±7.101; *Wdr62*$^{e2-/e2-}$ (*n*=76), 36.61±3.988; *Tnap-Cre* rescue (*n*=48), 87.38±3.118. Data are mean±s.e.m. from one experiment. ***P*<0.01 (Student's *t*-test, two-tailed).

DISCUSSION

WDR62 was originally identified as a JNK signaling scaffold protein that plays important roles in brain development (Chen et al., 2014; Cohen-Katsenelson et al., 2013, 2011; Verloes et al., 1993). The function of WDR62 in brain development has been investigated using a gene-trap mouse model. Homozygous mutant mice exhibited growth retardation and reduced brain size with spindle instability and mitotic arrest in neural progenitors and MEF cells. A mechanistic study demonstrated that WDR62 interacted with Aurora A to regulate spindle formation (Chen et al., 2014). Surprisingly, in the current study, we found that *Wdr62*$^{e2-/e2-}$ mice were born at a normal Mendelian ratio, and no obvious developmental defects were observed. Moreover, the proliferation and viability of MEF cells were not affected. This discrepancy is probably caused by the different strategies used to generate the mouse models. The gene trap mouse model was generated by inserting a β-geo reporter in the intron region between exons 14 and 15, which only caused a downregulation of WDR62 expression (Chen et al., 2014). By contrast, exon 2 was deleted in our mouse model, which caused a frame-shift of the *Wdr62* gene. Interestingly, a large isoform (~200-kD) of the WDR62 protein was detected in the testes, whereas it was absent in brain and MEF cells. By contrast, a small isoform (~170-kD) was detected in the brain, which was similar to the findings of a previous study (Lim et al., 2015b; Bogoyevitch et al., 2012). However, this small isoform was not recognized by the anti-HA antibody in *Wdr62-HA* mice. The large isoform (~200-kD) of the WDR62 protein has not been reported in previous work. Based on these results, we speculated that different isoforms of the *Wdr62* gene were expressed in the testes and brain. The small isoform probably terminates earlier, and thus, the HA tag was not translated. In our mouse model, the large isoform of WDR62 was deleted, but the small isoform was intact. The large and small isoforms of WDR62 most likely have different functions. The small isoform is involved in the development of neural progenitor cells and MEF cells, whereas the large isoform is important for germ cell meiosis. However, detailed information about the functions of these two isoforms requires further investigation.

It has been reported that WDR62 is required for spindle assembly and timely mitotic progression as a spindle pole protein which can be phosphorylated (Garcia-Higuera et al., 1996; Nawrot et al., 2006; Nicholas et al., 2010). An *in vitro* study also demonstrated that inactivation of *WDR62* in HeLa cells caused the defect of spindle orientation and delayed mitotic progression. A mechanistic study found that WDR62 was involved in spindle assembly in mitosis by interacting with JNK1 (Lim et al., 2015b; Bogoyevitch et al., 2012). A uterus electroporation study also found that WDR62 was involved in spindle assembly of rat neural progenitor cells by activating JNK signaling (Chen et al., 2014; Xu et al., 2014). Our previous study also found that the defect in female germ cell development was partially rescued by overexpression of JNK1 (Zhou et al., 2018). In this study, we found that inactivation of *Wdr62* also caused a defect in spindle assembly and centrosome positioning in germ cells, which in turn led to metaphase arrest of male germ cells. However, defective germ cell meiosis was not rescued by JNK1 overexpression, suggesting that the involvement of *Wdr62* in spindle assembly during meiosis of male germ cells is independent of JNK signaling.

Development (2019) 146, dev174128. doi:10.1242/dev.174128

The centrosome is the major microtubule organizing center and directs spindle assembly at metaphase in both meiosis and mitosis. It is composed of a pair of centrioles and embedded PCM (Gönczy, 2012; Sir et al., 2011). Centrosome proteins, such as CEP152, CEP63, CEP135 and CEP192, among others, are required for centriole duplication and spindle assembly in mitosis (Gomez-Ferreria and Sharp, 2008; Inanç et al., 2013; Kitagawa et al., 2011; Tang et al., 2011; Zhu et al., 2008). Inactivation of *Cep63* causes destruction of centriole duplication and impaired bipolar spindle assembly in meiosis (Marjanović et al., 2015). CEP170 is also a centrosome protein and localizes in subdistal appendages of the mature centriole to regulate spindle assembly and cell morphology (Guarguaglini et al., 2005). CEP170 interacts with the centrosome-associated kinesins KIF2A, KIF2C and KIFC3, and this complex plays an important role in metaphase spindle size control (Maliga et al., 2013). It also has been reported that WDR62 is a binding partner of CEP170 and other centrosomal proteins, and mutation of these genes is associated with microcephaly (Yu et al., 2010). In this study, we found that WDR62 was partially co-localized with CEP170, and the interaction between these two proteins was confirmed by Co-IP experiments. Most importantly, we found that the expression of CEP170 protein was dramatically reduced in *Wdr62*-deficient germ cells. Given that CEP170 is a centrosome protein and is involved in spindle assembly, we speculated that WDR62 is involved in spindle assembly, most likely by interacting with CEP170. Loss of *Wdr62* results in instability of the CEP170 protein, which in turn causes a defect of centrosome positioning and aberrant spindle assembly. However, we could not exclude the possibility that WDR62 is involved in spindle assembly by also interacting with other centrosome proteins or that it directly interacts with spindle proteins.

In mouse testis, a large number of germ cells directly start meiosis from gonocytes at ∼P3. This is considered the first wave of spermatogenesis. By contrast, a small number of gonocytes are transformed into spermatogonium, and spermatogenesis starts from these cells. Whether the meiosis of the first wave and the following spermatogenesis is regulated by similar mechanisms is unclear. The results of this and our previous study demonstrate that *Wdr62* has different roles in these two mechanisms. The meiosis of first-wave spermatogenesis is more similar to that seen in female germ cells. JNK signaling is involved in meiosis in female germ cells and the first wave of spermatogenesis, whereas it is not required for the following spermatogenesis. Another interesting finding was that the defect in germ cell survival in *Wdr62*-deficient mice was rescued by JNK1 overexpression, but the defect in spermatogenesis in juveniles and adults was not rescued. These results suggest that *Wdr62* plays different functions in germ cells at different developmental stages. In summary, we demonstrated that WDR62 played important roles in germ cell meiosis by interacting with CEP170. Loss of *Wdr62* resulted in downregulation of CEP170, which in turn caused an asymmetric distribution of the centrosome and aberrant spindle assembly. We also demonstrated that a large isoform of the *Wdr62* gene was specifically expressed in the testes and absent in the brain and other organs. This study provides new information that allows a better understanding of the regulation of germ cell meiosis progression and the functions of the *Wdr62* gene in different cell types.

MATERIALS AND METHODS

Mice

All mice studies were carried out in accordance with the principles approved by the Institutional Animal Care and Use Committee at the Institute of Zoology, Chinese Academy of Sciences. All mice were maintained in a C57BL/6; 129/SvEv mixed background. *Wdr62*$^{e2-/e2-}$ mice, *Wdr62-HA* mice, *Wdr62*$^{e2-/e2-}$*;CAJNK1*$^{+/flox}$*;Tnap-Cre* mice and *Wdr62*$^{e2-/e2-}$*; CAJNK1*$^{+/flox}$*;Stra8-Cre* mice were used in this research. See supplementary Materials and Methods for further details.

Tissue collection and histological analysis

Testes were dissected from control and mutant mice immediately after euthanasia, fixed in 4% paraformaldehyde (PFA) for up to 24 h, stored in 70% ethanol and embedded in paraffin. Next, 5 µm-thick sections were prepared using a rotary microtome (Leica) and mounted on glass slides. After deparaffinization, sections were stained with H&E for histological analysis.

Immunohistochemistry (IHC) analysis

IHC was performed with at least three mice for each genotype using a Vectastain ABC (avidin-biotin-peroxidase) kit (Vector Laboratories) as recommended by the manufacturer and as described previously (Han et al., 2018). The slides were examined using a Nikon Microscope, and images were captured with a Nikon DS-Ril CCD camera.

Immunofluorescence (IF) analysis

After deparaffinization and antigen retrieval, the sections were blocked with 5% donkey serum at room temperature (RT) for 1 h, followed by incubating with a primary antibody for 1 h at RT or overnight at 4°C. After washing three times in 1× PBS buffer, the slides were incubated with the corresponding secondary antibody, fluorescent dye-conjugated-FITC or TRITC (1:150, Jackson) for 1 h at RT. The nucleus was stained with DAPI. All images were captured with a confocal laser scanning microscope (Leica SP8 fitted with hybrid detectors).

Preparation of synaptonemal complex

The testes were dissected and seminiferous tubules were washed in 1× PBS buffer. After incubation with hypo extraction buffer (HEB) for 30 min, the tubules were disrupted in 0.1 M sucrose to make a cell suspension. The cell suspension was mounted on slides covered with 1% PFA. Slides were placed in a humidified box for at least 6 h. Then, the slides were air dried at RT for 30 min, washed in 0.04% Photo-Flo (Equl, 1464510) for 4 min and set at an angle for 10 min to dry. The air-dried-slides were then prepared for synaptonemal complex staining of SYCP3. Slides were incubated with 1× antibody dilution buffer (ADB) at RT for 30 min, followed by incubating with SYCP3 antibody overnight at 37°C. After washing three times in 1× Tris buffer, saline (TBS), the slides were blocked with 1× ADB overnight at 4°C. Washing three times in cold 1× TBS buffer, the slides were incubated with the corresponding secondary antibody, fluorescent dye-conjugated-TRITC for 3 h at 37°C. All images were captured using a confocal laser scanning microscope (Leica SP8 fitted with hybrid detectors).

CRISPR/Cas9

The HA tag TACCCATACGATGTTCCAGATTACGCT was inserted in front of the stop codon, TGA, of the *Wdr62* gene. See supplementary Materials and Methods for further details.

Plasmids

Wdr62-HA cDNA was amplified from adult *Wdr62-HA* mouse testes by RT-PCR and cloned into Xho1 and Not1 restriction sites to generate pCMS.EGFP-Wdr62-HA. *Cep170-Flag* cDNA was amplified from adult C57 mouse testes by RT-PCR and cloned into Mlu1 and Not1 restriction sites to generate pCMS.EGFP.Flag-Cep170-Flag.

Cell culture and transfection

HeLa cells (3111C0001CCC000011) and 293 cells (3111C0001CCC000010) were purchased from National Infrastructure of Cell Line Resource. They were authenticated and tests showed no contamination. HeLa cells and 293 cells were cultured in DMEM (Invitrogen) supplemented with 10% fetal bovine serum and 1% penicillin/streptomycin and grown in a humidified 5% CO_2 environment at 37°C, and showed a healthy state (i.e. adherent and normal proliferation). Transfection was mediated with Lipofectamine® 3000

Development (2019) 146, dev174128. doi:10.1242/dev.174128

(Invitrogen) and fetal bovine serum-free DMEM medium (Invitrogen) according to the manufacturer's instructions.

Isolation of MEF cells

MEF cells were isolated from E13.5 embryos as described previously (Chen et al., 2014). See supplementary Materials and Methods for further details.

Cell proliferation assay

The relative number and viability of MEF cells were evaluated by MTT assays at 1, 2, 3, 4, 5 or 6 days. See supplementary Materials and Methods for further details.

Co-immunoprecipitation (Co-IP)

Plasmids (2.5 µg of each plasmid) were transfected into 293 cells. Forty-eight hours after transfection, cell extracts were prepared using lysis buffer [50 mM Tris-HCl (pH 7.5), 100 mM NaCl, 2 mM EDTA (pH 8.0), 1% (v/v) NP40, 2 mM PMSF] supplemented with protease inhibitors and phosphatase inhibitors. For Co-IP, ∼1000 µg protein was incubated for 2-4 h *in vitro* (and 12 h *in vivo*) at 4°C with 15 µl indicated monoclonal HA-agarose (Sigma-Aldrich, A2095) or Flag-agarose (Sigma-Aldrich). The immunoprecipitates were washed five times using cell lysis buffer and the bound protein complex eluted by 2× SDS-PAGE loading buffer and analyzed with western blotting as described previously (Fan et al., 2017).

Antibodies

The primary antibodies used were: anti-BUBR1 (1:200, Abcam, ab28193), anti-SYCP3 (1:200, Abcam, ab97672), anti-γ-H2AX (1:400, Millipore, 05-636), anti-RAD51 (1:25, Santa Cruz Biotechnology, sc-839), anti-RPA1 (1:300, Abcam, ab87272), anti-DMC1 (1:25, Santa Cruz Biotechnology, sc-22768), anti-MLH1 (1:200, Abcam, ab92312), anti-α-tubulin-FITC (1:100, Sigma-Aldrich, F2168), anti-γ-tubulin (1:400, Abcam, ab11316), anti-centrin (1:100, Millipore, 04-1624), anti-HA (1:400, MBL International, M180-3) and anti-FLAG (1:400, MBL International, M185-3L).

Spindle analysis

We cut 5-µm-thick sections of testes using a rotary microtome (Leica, MR2235). Sections were immunostained with anti-α-tubulin antibody (as in the IF analysis) and the spindles were captured using a confocal laser scanning microscope (Leica, TCS SP8). We then counted a similar number of spermatocytes with α-tubulin-positive spindles in control and $Wdr62^{e2-/e2-}$testes and measured the parameters of the spindles, including the length, width and the intensity of α-tubulin.

Data and statistical analysis

All images were processed with Photoshop CS6 (Adobe) and ImageJ (National Institutes of Health). All statistics were analyzed using Microsoft Excel and Prism software (GraphPad Software). All experiments were confirmed with at least three independent experiments, and three to five control or mutant testes were used for immunostaining. The quantitative results were presented as the mean±s.e.m. The significant difference was evaluated with *t*-test and χ^2 test. *P*-value < 0.05 was considered as significant.

Acknowledgements

We thank Shuguang Duo, from the Institute of Zoology, Chinese Academy of Sciences, for help with CRISPR/Cas9 experiments. We thank the proteomics facility of the Institute of Genetics and Developmental Biology, Chinese Academy of Sciences, for help with mass spectrometry analyses.

Competing interests

The authors declare no competing or financial interests.

Author contributions

Conceptualization: F.G.; Methodology: Y.Q., Y.Z., Z.S., B.X., M.C. (0000-0001-5074-2174), Y.L., A.B., X.Q., Y.W.; Software: Y.Z., M.C. (0000-0001-6577-6705), J.Z.; Formal analysis: Y.Q., W.M., Y.W.; Investigation: Y.Q.; Resources: F.G.; Data curation: Y.Q., Z.S.; Writing - original draft: Y.Q.; Writing - review & editing: F.G.; Supervision: F.G.; Project administration: Y.Q.; Funding acquisition: F.G.

Funding

This work was supported by the National Key R&D program funded by the Ministry of Science and Technology of the People's Republic of China (2018YFA0107700); the National Science Fund for Distinguished Young Scholars from the Chinese Academy of Sciences (81525011); the Strategic Priority Research Program of the Chinese Academy of Sciences (XDB19000000); and the National Natural Science Foundation of China (31601193 and 31671496).

Supplementary information

Supplementary information available online at
http://dev.biologists.org/lookup/doi/10.1242/dev.174128.supplemental

References

Barroca, V., Lassalle, B., Coureuil, M., Louis, J. P., Le Page, F., Testart, J., Allemand, I., Riou, L. and Fouchet, P. (2009). Mouse differentiating spermatogonia can generate germinal stem cells in vivo. *Nat. Cell Biol.* **11**, 190-196. doi:10.1038/ncb1826

Baudat, F., Imai, Y. and de Massy, B. (2013). Meiotic recombination in mammals: localization and regulation. *Nat. Rev. Genet.* **14**, 794-806. doi:10.1038/nrg3573

Blobel, C. P. (2000). Functional processing of fertilin: evidence for a critical role of proteolysis in sperm maturation and activation. *Rev. Reprod.* **5**, 75-83. doi:10.1530/ror.0.0050075

Bogoyevitch, M. A., Yeap, Y. Y. C., Qu, Z., Ngoei, K. R., Yip, Y. Y., Zhao, T. T., Heng, J. I. and Ng, D. C. H. (2012). WD40-repeat protein 62 is a JNK-phosphorylated spindle pole protein required for spindle maintenance and timely mitotic progression. *J. Cell Sci.* **125**, 5096-5109. doi:10.1242/jcs.107326

Braun, R. E. (2000). Temporal control of protein synthesis during spermatogenesis. *Int. J. Androl.* **23** Suppl. 2, 92-94. doi:10.1046/j.1365-2605.2000.00027.x

Brinster, R. L. and Zimmermann, J. W. (1994). Spermatogenesis following male germ-cell transplantation. *Proc. Natl. Acad. Sci. USA* **91**, 11298-11302. doi:10.1073/pnas.91.24.11298

Chen, J.-F., Zhang, Y., Wilde, J., Hansen, K. C., Lai, F. and Niswander, L. (2014). Microcephaly disease gene Wdr62 regulates mitotic progression of embryonic neural stem cells and brain size. *Nat. Commun.* **5**, 3885. doi:10.1038/ncomms4885

Cohen-Katsenelson, K., Wasserman, T., Khateb, S., Whitmarsh, A. J. and Aronheim, A. (2011). Docking interactions of the JNK scaffold protein WDR62. *Biochem. J.* **439**, 381-390. doi:10.1042/BJ20110284

Cohen-Katsenelson, K., Wasserman, T., Darlyuk-Saadon, I., Rabner, A., Glaser, F. and Aronheim, A. (2013). Identification and analysis of a novel dimerization domain shared by various members of c-Jun N-terminal kinase (JNK) scaffold proteins. *J. Biol. Chem.* **288**, 7294-7304. doi:10.1074/jbc.M112.422055

de Rooij, D. G. and Russell, L. D. (2000). All you wanted to know about spermatogonia but were afraid to ask. *J. Androl.* **21**, 776-798.

Fan, H.-Y. (2010). BubR1, a spindle assembly checkpoint protein in mammalian oocyte meiosis. *Cell Cycle* **9**, 1456-1465. doi:10.4161/cc.9.8.11405

Fan, J., Wang, Y., Liu, L., Zhang, H., Zhang, F., Shi, L., Yu, M., Gao, F. and Xu, Z. (2017). cTAGE5 deletion in pancreatic beta cells impairs proinsulin trafficking and insulin biogenesis in mice. *J. Cell Biol.* **216**, 4153-4164. doi:10.1083/jcb.201705027

Farag, H. G., Froehler, S., Oexle, K., Ravindran, E., Schindler, D., Staab, T., Huebner, A., Kraemer, N., Chen, W. and Kaindl, A. M. (2013). Abnormal centrosome and spindle morphology in a patient with autosomal recessive primary microcephaly type 2 due to compound heterozygous WDR62 gene mutation. *Orphanet J. Rare Dis.* **8**, 178. doi:10.1186/1750-1172-8-178

Garcia-Higuera, I., Fenoglio, J., Li, Y., Lewis, C., Panchenko, M. P., Reiner, O., Smith, T. F. and Neer, E. J. (1996). Folding of proteins with WD-repeats: comparison of six members of the WD-repeat superfamily to the G protein beta subunit. *Biochemistry* **35**, 13985-13994. doi:10.1021/bi9612879

Gomez-Ferreria, M. A. and Sharp, D. J. (2008). Cep192 and the generation of the mitotic spindle. *Cell Cycle* **7**, 1507-1510. doi:10.4161/cc.7.11.5957

Gönczy, P. (2012). Towards a molecular architecture of centriole assembly. *Nat. Rev. Mol. Cell Biol.* **13**, 425-435. doi:10.1038/nrm3373

Gorbsky, G. J. (2015). The spindle checkpoint and chromosome segregation in meiosis. *FEBS J.* **282**, 2471-2487. doi:10.1111/febs.13166

Guarguaglini, G., Duncan, P. I., Stierhof, Y. D., Holmström, T., Duensing, S. and Nigg, E. A. (2005). The forkhead-associated domain protein Cep170 interacts with Polo-like kinase 1 and serves as a marker for mature centrioles. *Mol. Biol. Cell* **16**, 1095-1107. doi:10.1091/mbc.e04-10-0939

Haines, J. W., Coster, M. and Bouffler, S. D. (2015). Impairment of the non-homologous end joining and homologous recombination pathways of DNA double strand break repair: impact on spontaneous and radiation-induced mammary and intestinal tumour risk in Apc min/+ mice. *DNA Repair (Amst)* **35**, 19-26. doi:10.1016/j.dnarep.2015.08.002

Han, F., Liu, C., Zhang, L., Chen, M., Zhou, Y., Qin, Y., Wang, Y., Chen, M., Duo, S., Cui, X. et al. (2018). Globozoospermia and lack of acrosome formation in GM130-deficient mice. *Cell Death Dis.* **8**, e2532. doi:10.1038/cddis.2016.414
Hartwell, L. H. and Weinert, T. A. (1989). Checkpoints: controls that ensure the order of cell cycle events. *Science* **246**, 629-634. doi:10.1126/science.2683079
Inanç, B., Pütz, M., Lalor, P., Dockery, P., Kuriyama, R., Gergely, F. and Morrison, C. G. (2013). Abnormal centrosomal structure and duplication in Cep135-deficient vertebrate cells. *Mol. Biol. Cell* **24**, 2645-2654. doi:10.1091/mbc.e13-03-0149
Jia, L., Kim, S. and Yu, H. (2013). Tracking spindle checkpoint signals from kinetochores to APC/C. *Trends Biochem. Sci.* **38**, 302-311. doi:10.1016/j.tibs.2013.03.004
Keeney, S., Lange, J. and Mohibullah, N. (2014). Self-organization of meiotic recombination initiation: general principles and molecular pathways. *Annu. Rev. Genet.* **48**, 187-214. doi:10.1146/annurev-genet-120213-092304
Kitagawa, D., Kohlmaier, G., Keller, D., Strnad, P., Balestra, F. R., Fluckiger, I. and Gonczy, P. (2011). Spindle positioning in human cells relies on proper centriole formation and on the microcephaly proteins CPAP and STIL. *J. Cell Sci.* **124**, 3884-3893. doi:10.1242/jcs.089888
Kohl, K. P. and Sekelsky, J. (2013). Meiotic and mitotic recombination in meiosis. *Genetics.* **194**, 327-334. doi:10.1534/genetics.113.150581
Kousar, R., Hassan, M. J., Khan, B., Basit, S., Mahmood, S., Mir, A., Ahmad, W. and Ansar, M. (2011). Mutations in WDR62 gene in Pakistani families with autosomal recessive primary microcephaly. *BMC Neurol.* **11**, 119. doi:10.1186/1471-2377-11-119
Lim, N. R., Yeap, Y. Y. C., Ang, C. S., Williamson, N. A., Bogoyevitch, M. A., Quinn, L. M. and Ng, D. C. H. (2015a). Aurora A phosphorylation of WD40-repeat protein 62 in mitotic spindle regulation. *Cell Cycle* **15**, 413-424. doi:10.1080/15384101.2015.1127472
Lim, N. R., Yeap, Y. Y. C., Zhao, T. T., Yip, Y. Y., Wong, S. C., Xu, D., Ang, C.-S., Williamson, N. A., Xu, Z., Bogoyevitch, M. A. et al. (2015b). Opposing roles for JNK and Aurora A in regulating the association of WDR62 with spindle microtubules. *J. Cell Sci.* **128**, 527-540. doi:10.1242/jcs.157537
Ma, C. J., Gibb, B., Kwon, Y. H., Sung, P. and Greene, E. C. (2017). Protein dynamics of human RPA and RAD51 on ssDNA during assembly and disassembly of the RAD51 filament. *Nucleic Acids Res.* **45**, 749-761. doi:10.1093/nar/gkw1125
Maliga, Z., Junqueira, M., Toyoda, Y., Ettinger, A., Mora-Bermúdez, F., Klemm, R. W., Vasilj, A., Guhr, E., Ibarlucea-Benitez, I., Poser, I. et al. (2013). A genomic toolkit to investigate kinesin and myosin motor function in cells. *Nat. Cell Biol.* **15**, 325-334. doi:10.1038/ncb2689
Marjanović, M., Sánchez-Huertas, C., Terré, B., Gómez, R., Scheel, J. F., Pacheco, S., Knobel, P. A., Martínez-Marchal, A., Aivio, S., Palenzuela, L. et al. (2015). CEP63 deficiency promotes p53-dependent microcephaly and reveals a role for the centrosome in meiotic recombination. *Nat. Commun.* **6**, 7676. doi:10.1038/ncomms8676
Miyamoto, T., Akutsu, S. N., Fukumitsu, A., Morino, H., Masatsuna, Y., Hosoba, K., Kawakami, H., Yamamoto, T., Shimizu, K., Ohashi, H. et al. (2017). PLK1-mediated phosphorylation of WDR62/MCPH2 ensures proper mitotic spindle orientation. *Hum. Mol. Genet.* **26**, 4429-4440. doi:10.1093/hmg/ddx330
Nawrot, M., Liu, T., Garwin, G. G., Crabb, J. W. and Saari, J. C. (2006). Scaffold proteins and the regeneration of visual pigments. *Photochem. Photobiol.* **82**, 1482-1488. doi:10.1111/j.1751-1097.2006.tb09803.x
Nicholas, A. K., Khurshid, M., Désir, J., Carvalho, O. P., Cox, J. J., Thornton, G., Kausar, R., Ansar, M., Ahmad, W., Verloes, A. et al. (2010). WDR62 is associated with the spindle pole and is mutated in human microcephaly. *Nat. Genet.* **42**, 1010-1014. doi:10.1038/ng.682
Romanienko, P. J. and Camerini-Otero, R. D. (2000). The mouse Spo11 gene is required for meiotic chromosome synapsis. *Mol. Cell* **6**, 975-987. doi:10.1016/S1097-2765(00)00097-6
Sacristan, C. and Kops, G. J. P. L. (2015). Joined at the hip: kinetochores, microtubules, and spindle assembly checkpoint signaling. *Trends Cell Biol.* **25**, 21-28. doi:10.1016/j.tcb.2014.08.006
Shohayeb, B., Lim, N. R., Ho, U., Xu, Z., Dottori, M., Quinn, L. and Ng, D. C. H. (2017). The role of WD40-repeat protein 62 (MCPH2) in brain growth: diverse molecular and cellular mechanisms required for cortical development. *Mol. Neurobiol.* **55**, 5409-5424. doi:10.1007/s12035-017-0778-x
Sir, J.-H., Barr, A. R., Nicholas, A. K., Carvalho, O. P., Khurshid, M., Sossick, A., Reichelt, S., D'Santos, C., Woods, C. G. and Gergely, F. (2011). A primary microcephaly protein complex forms a ring around parental centrioles. *Nat. Genet.* **43**, 1147-1153. doi:10.1038/ng.971
Smirnova, N. A., Romanienko, P. J., Khil, P. P. and Camerini-Otero, R. D. (2006). Gene expression profiles of Spo11−/− mouse testes with spermatocytes arrested in meiotic prophase I. *Reproduction.* **132**, 67-77. doi:10.1530/rep.1.00997
Stirnimann, C. U., Petsalaki, E., Russell, R. B. and Müller, C. W. (2010). WD40 proteins propel cellular networks. *Trends Biochem. Sci.* **35**, 565-574. doi:10.1016/j.tibs.2010.04.003
Subramanian, V. V. and Hochwagen, A. (2014). The meiotic checkpoint network: step-by-step through meiotic prophase. *Cold Spring Harb. Perspect. Biol.* **6**, a016675. doi:10.1101/cshperspect.a016675
Tang, C.-J. C., Lin, S.-Y., Hsu, W.-B., Lin, Y.-N., Wu, C.-T., Lin, Y.-C., Chang, C.-W., Wu, K.-S. and Tang, T. K. (2011). The human microcephaly protein STIL interacts with CPAP and is required for procentriole formation. *EMBO J.* **30**, 4790-4804. doi:10.1038/emboj.2011.378
Tarsounas, M., Morita, T., Pearlman, R. E. and Moens, P. B. (1999). RAD51 and DMC1 form mixed complexes associated with mouse meiotic chromosome cores and synaptonemal complexes. *J. Cell Biol.* **147**, 207-220. doi:10.1083/jcb.147.2.207
Verloes, A., Drunat, S., Gressens, P. and Passemard, S. (1993). Primary autosomal recessive Microcephalies and Seckel syndrome spectrum disorders. In *GeneReviews* (ed. M. P. Adam, H. H. Ardinger, R. A. Pagon, S. E. Wallace, L. J. H. Bean, H. C. Mefford, K. Stephens, A. Amemiya and N. Ledbetter). University of Washington, Seattle.
Wasserman, T., Katsenelson, K., Daniliuc, S., Hasin, T., Choder, M. and Aronheim, A. (2010). A novel c-Jun N-terminal kinase (JNK)-binding protein WDR62 is recruited to stress granules and mediates a nonclassical JNK activation. *Mol. Biol. Cell* **21**, 117-130. doi:10.1091/mbc.e09-06-0512
Wei, L., Liang, X.-W., Zhang, Q.-H., Li, M., Yuan, J., Li, S., Sun, S.-C., Ouyang, Y.-C., Schatten, H. and Sun, Q.-Y. (2010). BubR1 is a spindle assembly checkpoint protein regulating meiotic cell cycle progression of mouse oocyte. *Cell Cycle* **9**, 1112-1121. doi:10.4161/cc.9.6.10957
Welburn, J. P. I. and Cheeseman, I. M. (2012). The microtubule-binding protein Cep170 promotes the targeting of the kinesin-13 depolymerase Kif2b to the mitotic spindle. *Mol. Biol. Cell* **23**, 4786-4795. doi:10.1091/mbc.e12-03-0214
Woglar, A. and Jantsch, V. (2014). Chromosome movement in meiosis I prophase of Caenorhabditis elegans. *Chromosoma.* **123**, 15-24. doi:10.1007/s00412-013-0436-7
Wollnik, B. (2010). A common mechanism for microcephaly. *Nat. Genet.* **42**, 923-924. doi:10.1038/ng1110-923
Xiong, B., Li, S., Ai, J.-S., Yin, S., Ouyang, Y.-C., Sun, S.-C., Chen, D.-Y. and Sun, Q.-Y. (2008). BRCA1 is required for meiotic spindle assembly and spindle assembly checkpoint activation in mouse oocytes. *Biol. Reprod.* **79**, 718-726. doi:10.1095/biolreprod.108.069641
Xu, X.-L., Ma, W., Zhu, Y.-B., Wang, C., Wang, B.-Y., An, N., An, L., Liu, Y., Wu, Z.-H. and Tian, J.-H. (2012). The microtubule-associated protein ASPM regulates spindle assembly and meiotic progression in mouse oocytes. *PLoS ONE* **7**, e49303. doi:10.1371/journal.pone.0049303
Xu, D., Zhang, F., Wang, Y., Sun, Y. and Xu, Z. (2014). Microcephaly-associated protein WDR62 regulates neurogenesis through JNK1 in the developing neocortex. *Cell Rep.* **6**, 1176-1177. doi:10.1016/j.celrep.2014.03.021
Xu, Z., Song, Z., Li, G., Tu, H., Liu, W., Liu, Y., Wang, P., Wang, Y., Cui, X., Liu, C. et al. (2016). H2B ubiquitination regulates meiotic recombination by promoting chromatin relaxation. *Nucleic Acids Res.* **44**, 9681-9697. doi:10.1093/nar/gkw652
Yamamoto, A. (2014). Gathering up meiotic telomeres: a novel function of the microtubule-organizing center. *Cell. Mol. Life Sci.* **71**, 2119-2134. doi:10.1007/s00018-013-1548-1
Yu, Z., Guo, R., Ge, Y., Ma, J., Guan, J., Li, S., Sun, X., Xue, S. and Han, D. (2003). Gene expression profiles in different stages of mouse spermatogenic cells during spermatogenesis. *Biol. Reprod.* **69**, 37-47. doi:10.1095/biolreprod.102.012609
Yu, T. W., Mochida, G. H., Tischfield, D. J., Sgaier, S. K., Flores-Sarnat, L., Sergi, C. M., Topçu, M., McDonald, M. T., Barry, B. J., Felie, J. M. et al. (2010). Mutations in WDR62, encoding a centrosome-associated protein, cause microcephaly with simplified gyri and abnormal cortical architecture. *Nat. Genet.* **42**, 1015-1020. doi:10.1038/ng.683
Yuan, J., Xu, B.-Z., Qi, S.-T., Tong, J.-S., Wei, L., Li, M., Ouyang, Y.-C., Hou, Y., Schatten, H. and Sun, Q.-Y. (2010). MAPK-activated protein kinase 2 is required for mouse meiotic spindle assembly and kinetochore-microtubule attachment. *PLoS ONE* **5**, e11247. doi:10.1371/journal.pone.0011247
Zhou, Y., Qin, Y., Qin, Y., Xu, B., Guo, T., Ke, H., Chen, M., Zhang, L., Han, F., Li, Y. et al. (2018). Wdr62 is involved in female meiotic initiation via activating JNK signaling and associated with POI in humans. *PLoS Genet.* **14**, e1007463. doi:10.1371/journal.pgen.1007463
Zhu, F., Lawo, S., Bird, A., Pinchev, D., Ralph, A., Richter, C., Müller-Reichert, T., Kittler, R., Hyman, A. A. and Pelletier, L. (2008). The mammalian SPD-2 ortholog Cep192 regulates centrosome biogenesis. *Curr. Biol.* **18**, 136-141. doi:10.1016/j.cub.2007.12.055

Supplementary Information

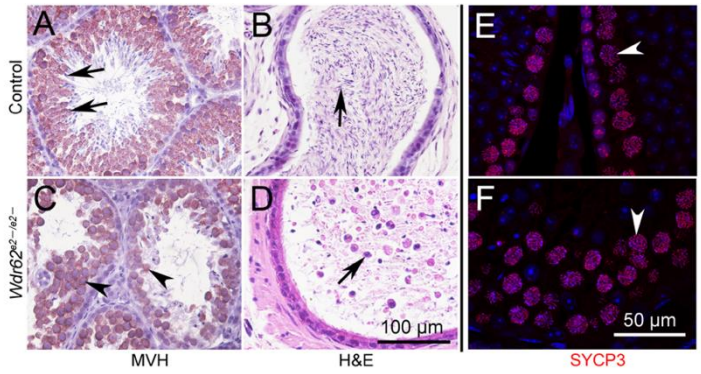

Fig. S1. Related to Fig. 1. Germ cells were arrested at the spermatocyte stage, and no mature sperm were observed in the epididymides of *Wdr62*-deficient mice. A large number of germ cells (C, black arrowheads) were observed in the seminiferous tubules of *Wdr62*$^{e2-/e2-}$ mice at 2 months of age, whereas no round/elongated spermatids were detected as in control testes (A, black arrows). The epididymides of control mice were filled with mature sperm (B, black arrows), whereas only cell debris was observed in *Wdr62*$^{e2-/e2-}$ mice (D, black arrows). A single layer of SYCP3-positive spermatocytes was observed in control testes (E, white arrowheads), whereas most of the germ cells in the seminiferous tubules of *Wdr62*$^{e2-/e2-}$ mice were SYCP3-positive (F, white arrowheads).

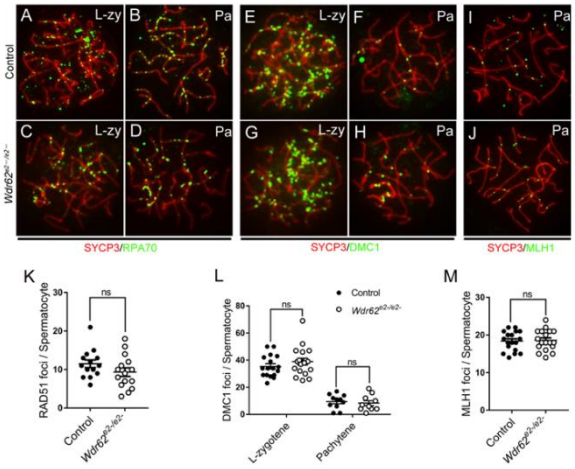

Fig. S2. Related to Fig. 2. No defect of DNA homologous recombination was observed in *Wdr62*-deficient germ cells. RPA70-positive foci (green) were detected on the chromosomes (red) of both control (A, B) and *Wdr62*-deficient (C, D) germ cells in the late zygotene (A, C) and pachytene (B, D) stages, and no difference was observed between control and *Wdr62*-deficient mice. A large number of DMC1-positive foci (green) were detected on the chromosomes (red) of both control (E, F) and *Wdr62*-deficient (G, H) germ cells in the late zygotene stage (E, G), and the number of foci (green) was dramatically reduced in the pachytene (F, H) stage in both control and *Wdr62*-deficient germ cells. Foci of the MLH1 protein (green) were observed in both control (I) and *Wdr62*$^{e2-/e2-}$ (J) germ cells at pachytene (I, J) stage. Quantification of the RAD51 foci per cell in control and *Wdr62*$^{e2-/e2-}$ mice at pachytene stage (K). Control (n=14), 11.5 ± 0.9931; *Wdr62*$^{e2-/e2-}$ (n=15) 9.333 ± 1.12. Quantification of the DMC1 foci per cell in control and *Wdr62*$^{e2-/e2-}$ mice at late-zygotene and pachytene stage (L). Late-zygotene: Control (n=17), 35.41±1.95; *Wdr62*$^{e2-/e2-}$ (n=18) 38.94 ± 2.526. Pachytene: Control (n=11), 9.455 ± 1.598; *Wdr62*$^{e2-/e2-}$ (n=10) 8.3 ± 1.844. Quantification of the MLH1 foci per cell in control and *Wdr62*$^{e2-/e2-}$ mice at pachytene stage (M). Control (n=18),18.39±0.6111; *Wdr62*$^{e2-/e2-}$ (n=18) 18.61±0.6424. The quantitative results were presented as the mean ± SEM from one experiment as the indicated number of cells. The significant difference was evaluated with *t*-test. P-value＞0.05 was considered as nonsense.

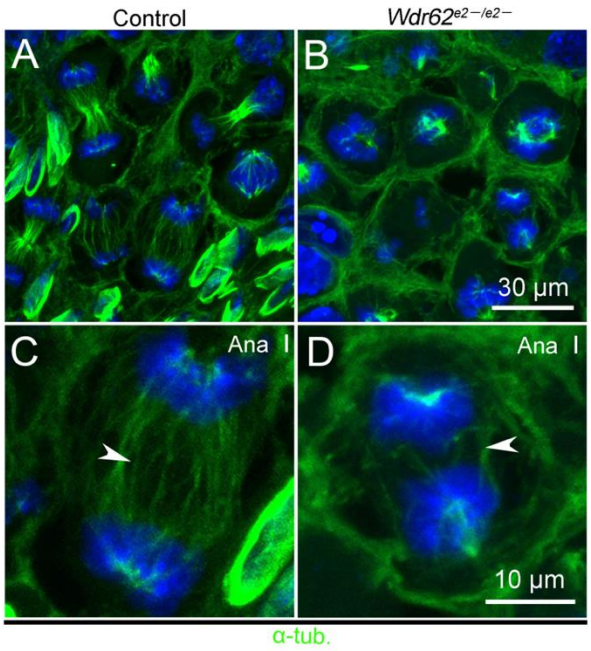

Fig. S3. Related to Fig. 4. Abnormal separation of chromosomes at anaphase I **in *Wdr62*-deficient germ cells**. In control mice, homologous chromosomes were separated at anaphase I with well-organized intermediate tubules (A, C, white arrowheads). Very few spermatocytes in anaphase I was observed in *Wdr62*$^{e2-/e2-}$ mice, and the intermediate tubules (B, D, white arrowheads) were seriously disrupted.

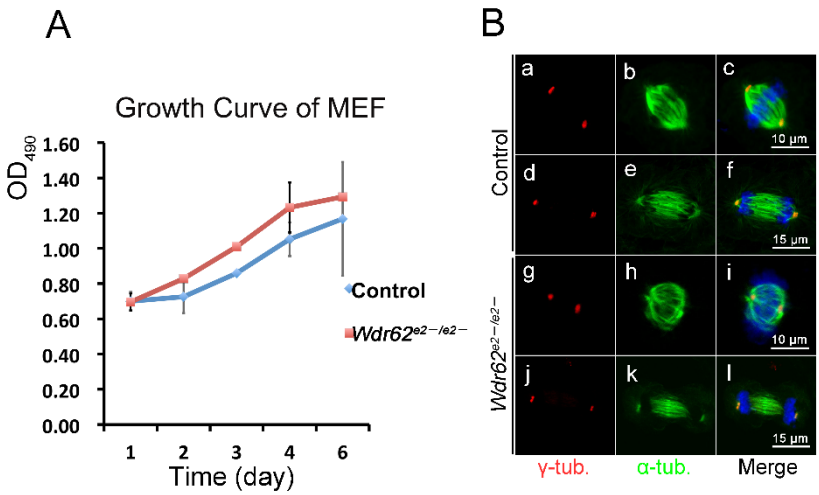

Fig. S4. Related to Fig. 5. The proliferation and spindle morphology of *Wdr62*-deficient MEF cells were not affected. MEF cells from control and *Wdr62*$^{e2-/e2-}$ mice were cultured *in vitro*, and the proliferation was examined by MTT assay. No difference in cell number and viability was observed between control and *Wdr62*-deficient MEF cells (A). The experiments were performed with three independent pools. The quantitative results were presented as the mean ± SEM. The significant difference was evaluated with *t*-test. P-value $>$ 0.05 was considered as nonsense. The morphology of the spindle and centrosome were examined by immunostaining (B). A well-organized spindle and a polar positioned centrosome in both control (a–f) and *Wdr62*-deficient (g–l) MEFs at metaphase (a–c, g–i) and anaphase (d–f, j–l) were observed.

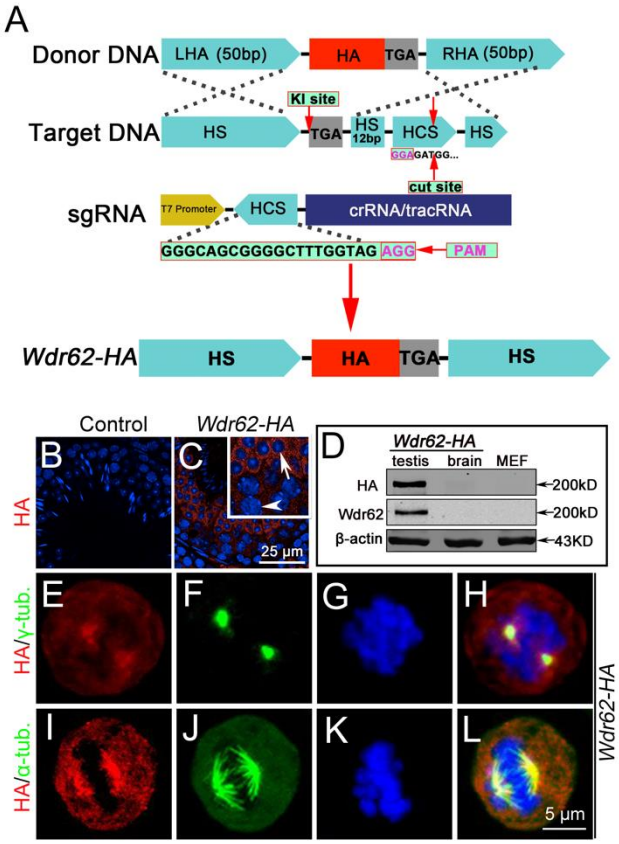

Fig. S5. Related to Fig. 6. WDR62 was abundantly expressed in spermatocytes/ spermatids and co-localized with the centrosome and spindle. (A) Schematic diagram for the generation of HA-tagged *Wdr62* knock-in mouse model using the CRISPR/Cas9 system. LHA/RHA, left/right homologous arms; HS, homologous sequences; HCS, homologous complementary sequence of gRNA; the protospacer-adjacent motif (PAM) sequence is labeled in pink; and the stop codon of *Wdr62* gene is labeled in the gray box. The results of immunofluorescence with anti-HA antibody showed *Wdr62* was highly expressed in spermatocytes (C, white arrowheads) and round spermatids (C, white arrows). WDR62 protein (~200 kD) was detected by western blot in the testes using both anti-HA and anti-WDR62 antibodies, but not in the brains and MEFs (D). WDR62 protein was localized in the cytoplasm of spermatocytes and co-localized with the centrosome (E–H) and spindle (I–L) at metaphase I.

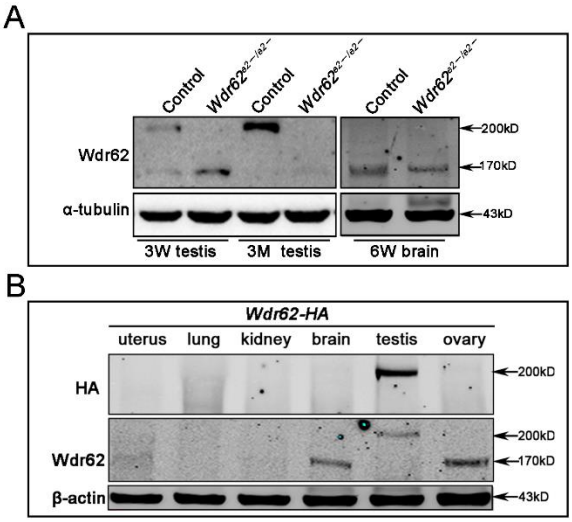

Fig. S6. Related to Fig. 6. The expression of different isoforms of the *Wdr62* gene in testes and other tissues. (A) A small (~170 kD) and a large (~200 kD) isoforms of protein were detected in the testes at 3 weeks by an anti-WDR62 antibody, but the large isoform was absent in *Wdr62*$^{e2-/e2-}$ testes. Only the large (~200 kD) isoform was detected in the testes at 3 months and was absent in *Wdr62*$^{e2-/e2-}$ testes. (B) The large isoform was only detected in adult testes by both anti-WDR62 and anti-HA antibodies. The small isoform was detected in the brain and ovary, but was not recognized by the anti-HA antibody.

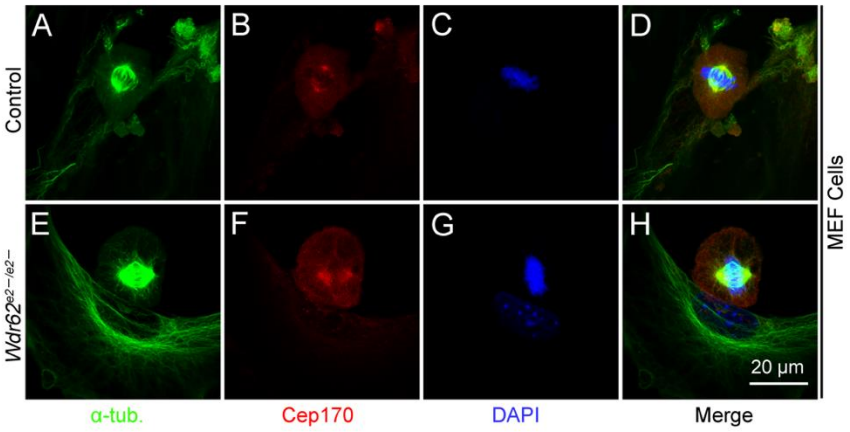

Fig. S7. Related to Fig. 6. The CEP170 positioning and spindle assembly of *Wdr62*-deficient MEF cells were not affected. A well-organized spindle and symmetrically located α-tubulin-positive spindles were observed in both control (A, D) and *Wdr62*-deficient (E, H) MEFs at metaphase (C, G). CEP170 protein was localized at the centrosome in control (B) and *Wdr62*-deficient (F) MEF cells.

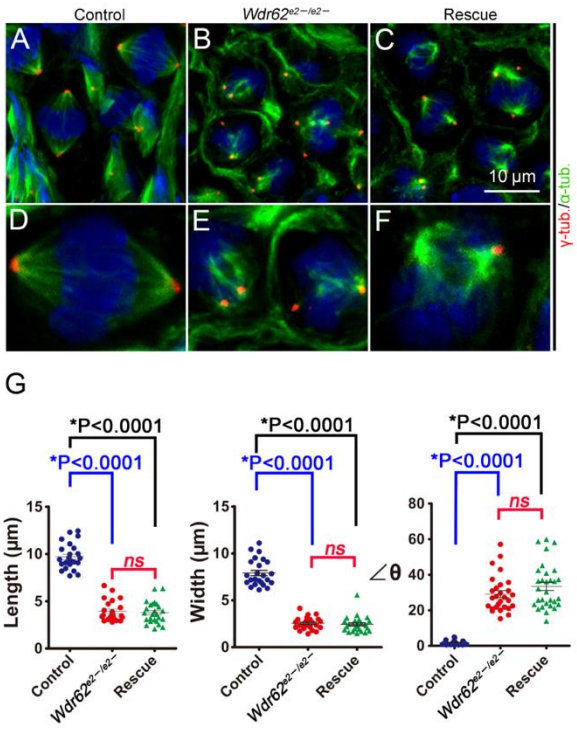

Fig. S8. Related to Fig. 8. The abnormality of spindle assembly in spermatocytes of *Wdr62*$^{e2-/e2-}$ mice was not rescued by JNK1 overexpression. Spindle and centrosome were labeled with anti-α-tubulin (green) and anti-γ-tubulin (red) antibodies. Compared with control (A, D), the polarity of the centrosome and structure of spindle were severely disrupted in *Wdr62*$^{e2-/e2-}$ mice (B, E), and this defect was not rescued in *Wdr62*$^{e2-/e2-}$*; CAJNK1*$^{+/flox}$*; Tnap-Cre* mice (Rescue) (C, F). (G) The quantitative analysis of the morphology of the spindle of spermatocytes at metaphase I in control, *Wdr62*$^{e2-/e2-}$, and Rescue mice. Count similar number of spermatocytes with α-tubulin-positive spindles in control, *Wdr62*$^{e2-/e2-}$ and Rescue testes, measure the parameters of spindles. Data are the mean ± SEM from one experiment with the indicated number of spermatocytes at Meta I (*p<0.0001) (Student's t-test).

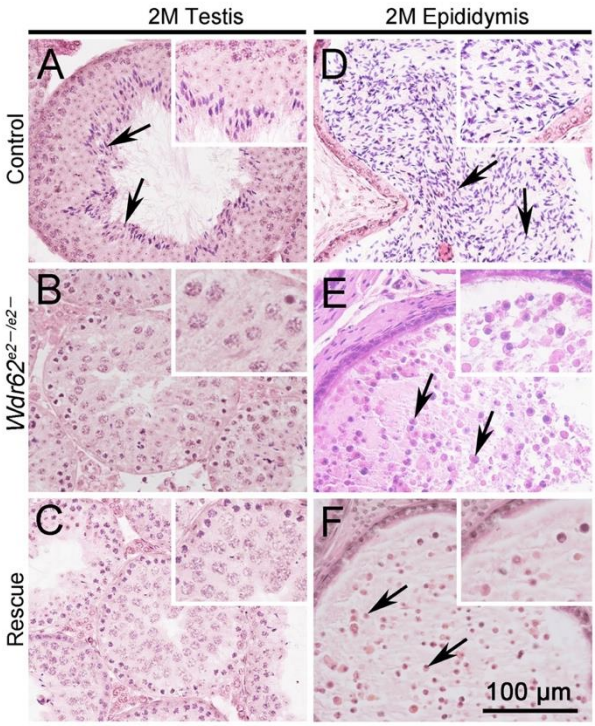

Fig. S9. Related to Fig. 8. The defect of spermatogenesis was not rescued in *Wdr62*$^{e2-/e2-}$; *CAJNK1*$^{+/flox}$; *Stra8-Cre* mice. Round and elongated spermatids were observed in control testes (A, black arrows), but only spermatocytes were observed in the seminiferous tubules of both *Wdr62*$^{e2-/e2-}$ (B, black arrowheads) and *Wdr62*$^{e2-/e2-}$; *CAJNK1*$^{+/flox}$; *Stra8-Cre* (C, black arrowheads) mice. Numerous mature sperm were observed in the epididymides of control mice (D, black arrows), but only cell debris was observed in the epididymides of *Wdr62*$^{e2-/e2-}$ (E, black arrows) and *Wdr62*$^{e2-/e2-}$; *CAJNK1*$^{+/flox}$; *Stra8-Cre* (F, black arrows) mice. Scale bars: 100 μm.

Supplementary Materials and methods

Mice

Wdr62$^{e2-/e2-}$ mice were obtained by crossing of *Wdr62*$^{+/e2-}$ mice. *Wdr62*$^{+/e2-}$ mice were generated as described previously (Zhou et al., 2018). The *Wdr62-HA* mouse lines were generated using CRISPR/Cas9 technology. *R26-JNKK2-JNK1 (JNK)* mice were acquired from Dr. Clive R Da Costa (Mammalian Genetics Laboratory, London Research Institute). *Wdr62*$^{e2-/e2-}$*;CAJNK1*$^{+/flox}$*;Tnap-Cre* mice and *Wdr62*$^{e2-/e2-}$*;CAJNK1*$^{+/flox}$*;Stra8-Cre* mice were generated by crossing *Wdr62*$^{+/e2-}$*;CAJNK1*$^{+/flox}$ mice with *Wdr62*$^{+/e2-}$*;Tnap-Cre* mice or *Wdr62*$^{+/e2-}$*;Stra8-Cre* mice. Genotyping (Gao et al., 2006; Higashino et al., 1999) was performed by PCR using DNA isolated from the tail tips of mice at 2 weeks. The tail tips were digested in 100 μL Solution A (25 mM NaOH + 0.2 mM EDTA) at 95℃ for 1 hour, followed with adding 100 μL Solution B (40 mM Tris-HCl).

Isolation of MEF cells

The embryos were dissected from control and mutant pregnant mice at E13.5 immediately after euthanasia, and washed in 1×PBS for three times. Then, transferred into serum-free medium and removed guts, head and limbs. The remaining bodies were dissected in 6 cm dishes with 1 ml DMEM and then digested by adding 3 ml 0.25% trypsin (Sigma) in a water bath with circular agitation (100 rpm) at 37°C for 15 min. The digestion was stopped by adding equal volume of 10% FBS. The MEF cell suspension was plated in 10 cm dishes with 10 ml DMEM (Invitrogen) supplemented with 10% FBS and 1% penicillin/streptomycin and cultured in a humidified 5% CO_2 at 37 ℃ (Gilks et al., 2004; Jian-Fu Chen, 2014).

Cell proliferation assay

MEF cells were cultured in DMEM of 96-well plates at 4×10^3 cells/well and counted at 1, 2, 3, 4, 5 or 6 days as described above. A volume of 20 μL 5 mg/mL MTT (Sigma) was added to each well and incubated at 37 ℃ for 4 hours. The corresponding product formazan were dissolved in 200 μL DMSO and the absorbance was measured by spectrophotometrically at 490 nm (OD_{490}) using a multifunction enzyme-linked analyzer.

CRISPR/Cas9

A 130-bp Wdr62-HA donor DNA was synthesized by Sangon Biotech (Shanghai). sgRNA was designed as Cas9-direct in Zhang Feng's laboratory online website (http://crispr.mit.edu/). The ~200-bp sgRNA fragment was amplified by PCR and transcribed with a MEGAshortscriptTM Kit (Ambion, AM1354). The Cas9 plasmid was linearized with Xba1 and transcribed with mMESSAGE mMACHINE® T7 Ultra Kit (Ambion, AM1345). RNA purification was performed with MEGAclear™ Kit (Ambion, AM1908). Cas9/gRNA/donor DNA co-injection of one-cell embryo was performed as previously described (Ma et al., 2014; Shen et al., 2013). Genotyping was performed by PCR as described previously using the DNA from tail biopsies.

Supplementary references

Gao, F., Maiti, S., Alam, N., Zhang, Z., Deng, J.M., Behringer, R.R., Lecureuil, C., Guillou, F., and Huff, V. (2006). The Wilms tumor gene, Wt1, is required for Sox9 expression and maintenance of tubular architecture in the developing testis. *Proc Natl Acad Sci U S A.* 103, 11987-11992.

Gilks, N., Kedersha, N., Ayodele, M., Shen, L., Stoecklin, G., Dember, L.M., and Anderson, P. (2004). Stress granule assembly is mediated by prion-like aggregation of TIA-1. *Mol Biol Cell.* 15, 5383-5398.

Higashino, M., Harada, N., Hataya, I., Nishimura, N., Kato, M., and Niikawa, N. (1999). Trizygotic pregnancy consisting of two fetuses and a complete hydatidiform mole with dispermic androgenesis. *Am J Med Genet.* 82, 67-69.

Jian-Fu Chen, L.N. (2014). Microcephaly Disease Gene Wdr62 Regulates Mitotic Progression of Embryonic Neural Stem Cells and Brain Size. *Nat Commun.*

Ma, Y., Zhang, X., Shen, B., Lu, Y., Chen, W., Ma, J., Bai, L., Huang, X., and Zhang, L. (2014). Generating rats with conditional alleles using CRISPR/Cas9. *Cell Res.* 24, 122-125.

Shen, B., Zhang, J., Wu, H., Wang, J., Ma, K., Li, Z., Zhang, X., Zhang, P., and Huang, X. (2013). Generation of gene-modified mice via Cas9/RNA-mediated gene targeting. *Cell Res.* 23, 720-723.

Zhou, Y., Qin, Y., Qin, Y., Xu, B., Guo, T., Ke, H., Chen, M., Zhang, L., Han, F., Li, Y., *et al.* (2018). Wdr62 is involved in meiotic initiation via activating JNK signaling and associated with POI in humans. *PLoS Genet.* 14, e1007463.